Drug Design, Development and Therapy

Dovepress
open access to scientific and medical research

Open Access Full Text Article

ORIGINAL RESEARCH

In vitro and in vivo Biological Evaluation of Newly Tacrine-Selegiline Hybrids as Multi-Target Inhibitors of Cholinesterases and Monoamine Oxidases for Alzheimer's Disease

Shu-Tong Huang[1,2,*], Jin-Chong Luo[1,3,*], Guo-Hui Zhong[1,2], Li-Ping Teng[4], Cai-Yan Yang[4], Chun-Li Tang[1], Lin Jing[1], Zhong-Bo Zhou[4], Jing Liu[1,3], Neng Jiang[1,2]

[1]Department of Pharmacy, Guangxi Medical University Cancer Hospital, Nanning, Guangxi, People's Republic of China; [2]Pharmaceutical College, Guangxi Medical University, Nanning, Guangxi, People's Republic of China; [3]School of Pharmacy, Jiangxi University of Chinese Medicine, Nanchang, People's Republic of China; [4]School of Pharmacy, Youjiang Medical University for Nationalities, Baise, Guangxi, People's Republic of China

*These authors contributed equally to this work

Correspondence: Jing Liu, School of Pharmacy, Jiangxi University of Chinese Medicine, No. 56, Yangming Road, Donghu District, Nanchang, Jiangxi, 330006, People's Republic of China, Email liujing860828@163.com; Neng Jiang, Department of Pharmacy, Guangxi Medical University Cancer Hospital, 71 Hedi Road, Qingxiu District, Nanning, Guangxi, 530021, People's Republic of China, Tel/Fax +86-17307711726, Email cpujnh@163.com

Purpose: Alzheimer's disease (AD) is the most common neurodegenerative disease, and its multifactorial nature increases the difficulty of medical research. To explore an effective treatment for AD, a series of novel tacrine-selegiline hybrids with ChEs and MAOs inhibitory activities were designed and synthesized as multifunctional drugs.

Methods: All designed compounds were evaluated in vitro for their inhibition of cholinesterases (AChE/BuChE) and monoamine oxidases (MAO-A/B) along with their blood-brain barrier permeability. Then, further biological activities of the optimizing compound **7d** were determined, including molecular model analysis, in vitro cytotoxicity, acute toxicity studies in vivo, and pharmacokinetic and pharmacodynamic property studies in vivo.

Results: Most synthesized compounds demonstrated potent inhibitory activity against ChEs/MAOs. Particularly, compound **7d** exhibited good and well-balanced activity against ChEs (*h*AChE: IC_{50} = 1.57 μM, *h*BuChE: IC_{50} = 0.43 μM) and MAOs (*h*MAO-A: IC_{50} = 2.30 μM, *h*MAO-B: IC_{50} = 4.75 μM). Molecular modeling analysis demonstrated that **7d** could interact simultaneously with both the catalytic active site (CAS) and peripheral anionic site (PAS) of AChE in a mixed-type manner and also exhibits binding affinity towards BuChE and MAO-B. Additionally, **7d** displayed excellent permeability of the blood-brain barrier, and under the experimental conditions, it elicited low or no toxicity toward PC12 and BV-2 cells. Furthermore, **7d** was not acutely toxic in mice at doses up to 2500 mg/kg and could improve the cognitive function of mice with scopolamine-induced memory impairment. Lastly, **7d** possessed well pharmacokinetic characteristics.

Conclusion: In light of these results, it is clear that **7d** could potentially serve as a promising multi-functional drug for the treatment of AD.

Keywords: Alzheimer's disease, cholinesterase, monoamine oxidase, multi-target, designed

Introduction

Alzheimer's disease (AD) is an age-related, chronic, primary brain nervous system degenerative disorder, characterized by memory loss, cognitive dysfunction and behavioral abnormalities that gradually worsen over time and ultimately result in death.[1,2] The global number of AD cases had increased by 117% between 1990 and 2016 due to the aging of the population, with over 50 million people living with dementia today and a projected 152 million by 2050 according to the latest available data.[3] AD, being the leading cause of dementia and the only one of the top 10 lethal diseases worldwide

Received: 21 August 2023
Accepted: 15 January 2024
Published: 24 January 2024

Graphical Abstract

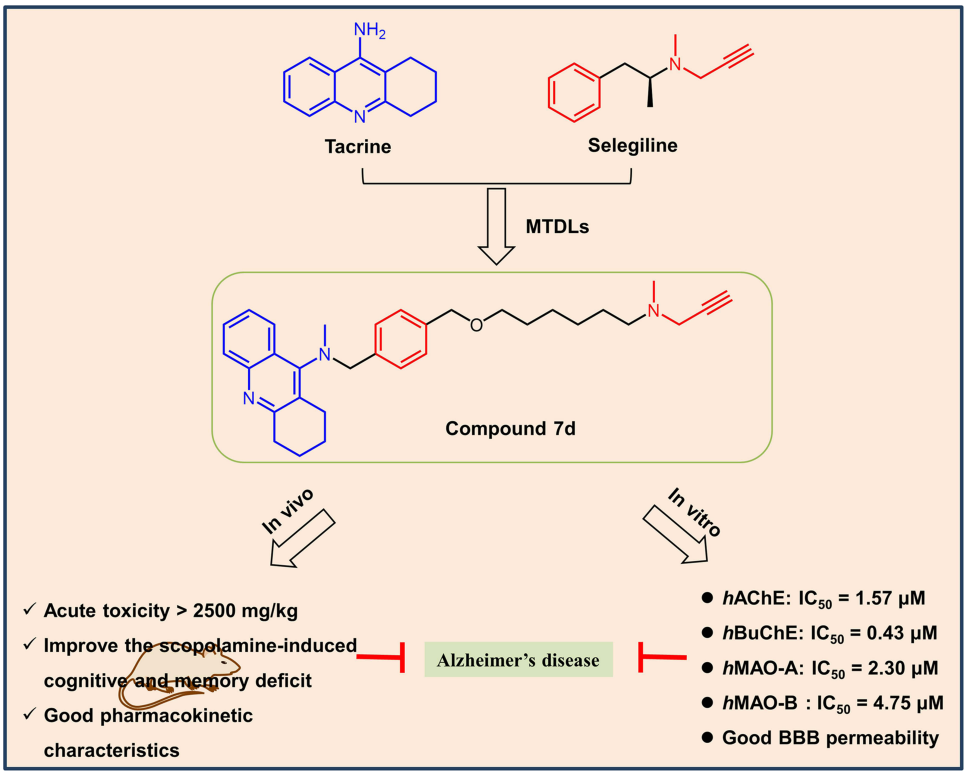

without an effective treatment, with care costs of around $1 trillion annually, is fast becoming one of the most expensive, deadly, and burdensome diseases of this century.[2,4,5] Despite the urgent need, AD drug development has experienced obstacles. AD is a multifactorial disease whose exact pathological causes are not yet fully understood. However, several factors, such as a deficit of acetylcholine (ACh)[6] and oxidative stress caused by increased activity of monoamine oxidase, play important roles in the pathogenesis of AD.[7–9] Although strong efforts are underway to elucidate the underlying mechanisms of the disease, translating these findings into novel therapeutic approaches remains challenging.

To date, the FDA has approved three types of drugs for the treatment of AD: three central AChE inhibitors (Donepezil, Rivastigmine and Galantamine), a partial antagonist of the *N*-methyl-D-aspartate (NMDA) receptor (Memantine),[10] and two anti-beta-amyloid (Aβ) monoclonal antibodies (Aducanumab and Lecanemab).[11] However, the approval of these two anti-amyloid antibodies is controversial, and further data are needed to confirm their effectiveness.[11] Thus, in deed, drug therapy for AD is primarily based on central AChE inhibitors to compensate for cholinergic defects in the brain.[12] A significant decrease of endogenous ACh in the brain can result in the typical pathological features of AD, such as cognitive decline.[13] AChE, mainly present in blood and synapses, is the principal enzyme responsible for the hydrolysis of acetylcholine (~90%) and is the most feasible therapeutic target for improving AD symptoms.[9,14] In addition to AChE, the liver also contains butyl cholinesterase (BuChE).[9] These two enzymes share almost 65% homologous amino acid sequences, and both possess a catalytic active site (CAS), a deep gorge and a peripheral anionic site (PAS).[15] BuChE serves as a crucial compensatory enzyme in progressed AD. When neurons undergo severe damage in patients with AD, the AChE level in the brain declines to 90% of the normal value, while the BuChE level can increase up to 120% of the physiological state.[5,15] Moreover, studies have suggested that the accumulation of BuChE in senile plaques is closely related to the progressive buildup of Aβ.[16] Therefore, BuChE can also be used as a drug target to treat AD. Tacrine (9-amino-1,2,3,4-tetrahydroacridine) was the first FDA-approved cholinesterase inhibitor for AD treatment but limited by hepatotoxicity and low bioavailability.[12,17] Nonetheless, it is

widely used in medicinal chemistry since it has good blood-brain barrier permeability, low molecular weight, synthesizability, and easy modification, serving as a scaffold for the development of new multifunctional drugs with minimal side effects.[18,19] In recent years, structural modifications of tacrine have mainly focused on substituting the benzene ring with a heterocycle and molecular hybridization based on tacrine.[12] Studies have revealed that homologous and heterodimers improve and extend the function of tacrine, while reducing side effects.[20,21]

Monoamine oxidases (MAOs) are flavoproteins that catalyze the oxidative deamination of monoamines (endogenous or exogenous). They are localized as dimers on the outer mitochondrial membrane and are classified into two subtypes, MAO-A and MAO-B, based on their acting substrates and selective inhibitors.[22] In the central nervous system (CNS), MAO-A is predominantly located in neuron axons and responsible for the oxidative deamination of a broad range of monoamine neurotransmitters, such as serotonin, norepinephrine, and epinephrine, while MAO-B is mainly expressed in glial cells and decomposes approximately 70% of dopamine.[22–24] Inhibitions of MAO-A have been approved for the treatment of neurasthenia, depression, and anxiety, while MAO-B inhibitors hold promise for the management of AD and Parkinson's disease (PD). With age, the expression level of MAO-B in the brain increases by up to fourfold, generating a massive number of free radicals that contribute to oxidative stress, which is identified as one of the pathogenic factors for AD.[25] Moreover, AD patients exhibit reduced concentrations of several monoamine neurotransmitters, including serotonin, dopamine, and norepinephrine.[26] These studies demonstrated that elevated MAO activity is closely related to the onset of AD. Therefore, MAO inhibitors, which slow the metabolism of monoamine neurotransmitters and exert indirect antioxidant effects by inhibiting MAO activity, have been identified as candidates for AD treatment. For instance, selegiline is an irreversible selective MAO-B inhibitor that shows neuroprotective effects in both in vitro and in vivo models of AD.[27]

Given the multifactorial nature of AD, single-target drugs often face difficulties in interfering with the complex network regulation of the disease and may produce high levels of toxicity. As a result, the development of multi-target directed ligands (MTDLs) has emerged as an important direction in current research, and multi-target drugs may be critical and effective in regulating the progression of AD. One of the most common approaches for the design of multi-target AD drugs involves pharmacophore conjugation, which combines two or more pharmacophores with known activities to form hybrid compounds. These hybrids not only inherit or amplify the anti-AD bioactivity of the parent compound but also offer the potential for lower side effects.[28] As ChEs and MAOs are two key targets for the treatment of AD, numerous multi-targeted drugs have been discovered and developed that target both enzymes.[21,28,29] One such drug is Ladostigil, a bifunctional agent that combines the carbamate moiety of rivastigmine and the indoleamine moiety of rasagiline. This drug has inhibitory activities on AChE, BuChE, MAO-A and MAO-B and has entered a phase IIb clinical trial,[30] indicating that the combination of ChEs and MAOs inhibitors is a promising method for the development of new multifunctional anti-AD drugs.

Inspired by the above concept of drug molecular design, a series of novel tacrine-selegiline hybrids with ChE and MAO inhibitory activities were designed and synthesized as multifunctional drugs against AD, based on tacrine (AChE and BuChE inhibitory activities) and selegiline (MAO-B inhibitory activity) (Figure 1). All designed compounds were synthesized and evaluated for their in vitro cholinesterase and monoamine oxidase inhibitory activities as well as their blood-brain barrier permeability. Furthermore, we performed molecular simulation studies, acute toxicity and neurotoxicity assessments, and pharmacokinetic and pharmacodynamic property evaluations for the optimizing compound.

Materials and Methods

Chemistry

Reagents and solvents were purchased from commercial suppliers (China) and used without additional purification. All reaction processes were monitored by analytical thin layer chromatography (TLC) on glass-packed pre-coated silica gel GF254 (Qingdao Haiyang Chemical Co., Ltd., China) plates under 254 nm UV light. Compounds were purified through column chromatography using silica gel (90–150 mm, Qingdao Marine Chemical Inc.) as the stationary phase and a mixture of PE/EA or DCM/MeOH as the elution system. The ^{1}H- (600 MHz) and ^{13}C- (150 MHz) NMR spectra at room temperature were recorded on a Bruker AVANCE-NEO 600 MHz spectrometer using CD_2Cl_2, $CDCl_3$, or DMSO-d_6 solvents. Chemical shifts (δ) are expressed in parts per million (ppm), and coupling constants (J) in hertz (Hz). High-resolution mass spectra (HRMS) were obtained with a Mariner ESI-TOF spectrometer (HRESIMS). After being characterized by ^{1}H NMR and HRMS, the intermediate undergoes the next

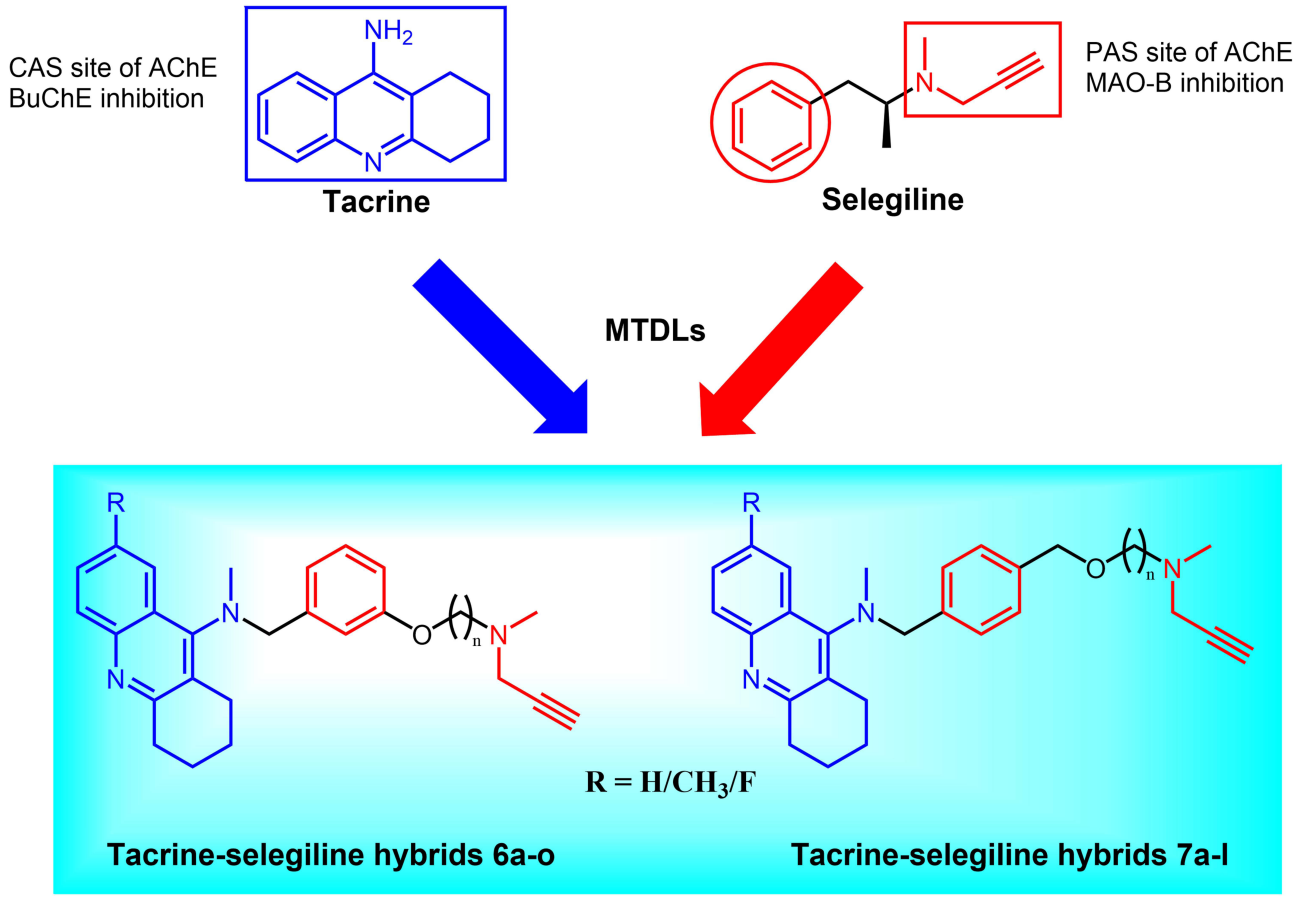

Figure 1 Design strategy toward tacrine-selegiline hybrids **6a-o** and **7a-l**.

reaction directly, while the target product was characterized using ^{1}H NMR, ^{13}C NMR, and HRMS. The samples of the tacrine-selegiline hybrids, which underwent pharmacological evaluation, possessed a purity > 95% as indicated by their high-performance liquid chromatography (HPLC) analyses.

Preparation of Intermediates 3a-3e

To a stirred solution of compound **1a-c** (6.89 mmol, 1.0 equiv.) and KI (0.34 mmol, 0.05 equiv.) in 1-pentanol (20 mL), compound **2a** 3-hydroxy benzylamine or **2b** 4-hydroxymethyl benzylamine (13.78mmol, 2.0 equiv.) was added and refluxed (130 °C) for 8–10 h.[31] After completion, it was concentrated to dryness, diluted with water, and extracted with EA (30 mL × 1, 20 mL × 3). The organic phase was washed with saturated salt water, dried with anhydrous sodium sulfate, filtered, and evaporated under reduced pressure. The crude product was purified by silica gel column chromatography (DCM/MeOH: 20/1~10/1, v/v) to give compounds **3a-3e**.

3-(((1,2,3,4-tetrahydroacridin-9-yl)amino)methyl)phenol (**3a**). Yield 51%; yellow solid; ^{1}H NMR (600 MHz, DMSO-d_6) δ 8.10 (d, J = 8.6 Hz, 1H), 7.70 (d, J = 8.5 Hz, 1H), 7.51 (q, J = 6.8 Hz, 1H), 7.28 (q, J = 6.7 Hz, 1H), 7.08 (q, J = 6.6, 5.8 Hz, 1H), 6.75 (d, J = 9.1 Hz, 2H), 6.61 (d, J = 8.1 Hz, 1H), 6.00 (d, J = 10.2 Hz, 1H), 4.56 (t, J = 5.5 Hz, 2H), 2.89 (q, J = 5.8 Hz, 2H), 2.72 (d, J = 6.1 Hz, 2H), 1.78 (dt, J = 20.4, 6.5 Hz, 4H) (Figure S1 in the Supporting Information); HRMS (ESI): m/z calcd for $C_{20}H_{21}N_2O$ $[M+H]^+$: 305.1648; found: 305.1691(Figure S2 in the Supporting Information).

3-(((7-methyl-1,2,3,4-tetrahydroacridin-9-yl)amino)methyl)phenol (**3b**). Yield 54%; yellow solid; ^{1}H NMR (600 MHz, DMSO-d_6) δ 9.36 (s, 1H), 7.90 (s, 1H), 7.60 (d, J = 8.5 Hz, 1H), 7.39–7.32 (m, 1H), 7.08 (t, J = 7.9 Hz, 1H), 6.75 (d, J = 7.2 Hz, 2H), 6.60 (dd, J = 8.1, 2.3 Hz, 1H), 6.11 (d, J = 7.6 Hz, 1H), 4.54 (d, J = 7.1 Hz, 2H), 2.86 (t, J = 6.3 Hz, 2H), 2.69 (t, J = 6.2 Hz, 2H), 2.38 (s, 3H), 1.82–1.70 (m, 4H) (Figure S3 in the Supporting Information); HRMS (ESI): m/z calcd for $C_{21}H_{23}N_2O$ $[M+H]^+$: 319.1805; found: 319.1860 (Figure S4 in the Supporting Information).

3-(((7-fluoro-1,2,3,4-tetrahydroacridin-9-yl)amino)methyl)phenol (**3c**). Yield 72%; yellow solid; ^{1}H NMR (600 MHz, DMSO-d_6) δ 9.33 (s, 1H), 7.86 (dd, J = 11.4, 2.8 Hz, 1H), 7.75 (dd, J = 9.2, 5.8 Hz, 1H), 7.42 (td, J = 8.6, 2.7 Hz, 1H), 7.08 (t, J = 8.0 Hz, 1H), 6.73 (dd, J = 4.4, 2.3 Hz, 2H), 6.59 (dd, J = 8.1, 2.3 Hz, 1H), 6.15 (s, 1H), 4.51 (d, J = 7.1 Hz, 2H), 2.88 (t, J = 6.4 Hz, 2H), 2.72 (t, J = 6.3 Hz, 2H), 1.82–1.70 (m, 4H) (Figure S5 in the Supporting Information); HRMS (ESI): m/z calcd for $C_{20}H_{20}FN_2O[M+H]^+$: 323.1554; found: 323.1588 (Figure S6 in the Supporting Information).

(4-(((1,2,3,4-tetrahydroacridin-9-yl)amino)methyl)phenyl)methanol (**3d**). Yield 77%; yellow solid; ^{1}H NMR (600 MHz, Methylene Chloride-d_2) δ 7.99 (dd, J = 8.5, 1.4 Hz, 1H), 7.83 (dd, J = 8.5, 1.3 Hz, 1H), 7.54 (ddd, J = 8.3, 6.8, 1.4 Hz, 1H), 7.37–7.30 (m, 5H), 4.68 (s, 2H), 4.64–4.57 (m, 2H), 4.24 (s, 1H), 3.00 (t, J = 6.2 Hz, 2H), 2.66 (t, J = 6.2 Hz, 2H), 1.90–1.83 (m, 4H) (Figure S7 in the Supporting Information); HRMS (ESI): m/z calcd for $C_{21}H_{23}N_2O$ $[M+H]^+$: 319.1805; found: 319.1858 (Figure S8 in the Supporting Information).

(4-(((7-methyl-1,2,3,4-tetrahydroacridin-9-yl)amino)methyl)phenyl)methanol (**3e**). Yield 62%; yellow solid; ^{1}H NMR (600 MHz, DMSO-d_6) δ 8.25 (s, 1H), 8.12 (s, 1H), 7.84 (d, J = 8.6 Hz, 1H), 7.60 (d, J = 8.6 Hz, 1H), 7.33 (d, J = 7.9 Hz, 2H), 7.29 (d, J = 7.9 Hz, 2H), 5.02 (d, J = 6.7 Hz, 2H), 4.46 (s, 2H), 2.98 (d, J = 5.2 Hz, 2H), 2.72 (d, J = 5.1 Hz, 2H), 2.34 (s, 3H), 1.79 (t, J = 3.6 Hz, 4H) (Figure S9 in the Supporting Information); HRMS (ESI): m/z calcd for $C_{22}H_{25}N_2O$ $[M+H]^+$: 333.1961; found: 333.2015 (Figure S10 in the Supporting Information).

General Procedure for the Preparation of Compounds 4a-4e

A mixture of intermediate **3a-3e** (4.24 mmol, 1.0 equiv.), 40% formaldehyde solution (14.84mmol, 3.5 equiv.), and glacial acetic acid (4.24 mmol, 1.0 equiv.) in DMF (30 mL) was stirred at room temperature for 60 min, then sodium cyanoborohydride (12.72 mmol, 3.0 equiv.) was added and stirred at room temperature for 8 h.[32] After completion, the mixture was poured into appropriate water and extracted with EA (20 mL × 3, 10 mL × 1). The organic phase was washed with saturated salt water, dried with anhydrous Na_2SO_4, filtered, and concentrated in a vacuum. The residue was purified by silica gel chromatography (PE/EA: 1/1~1/3, v/v), and compounds **4a-4e** were obtained.

3-((methyl(1,2,3,4-tetrahydroacridin-9-yl)amino)methyl)phenol (**4a**). Yield 78%; yellow solid; ^{1}H NMR (600 MHz, DMSO-d_6) δ 9.31 (s, 1H), 8.09 (d, J = 8.4 Hz, 1H), 7.89 (d, J = 8.4 Hz, 1H), 7.67 (s, 1H), 7.52 (s, 1H), 7.13 (t, J = 8.0 Hz, 1H), 6.75–6.70 (m, 2H), 6.67 (dd, J = 8.1, 2.4 Hz, 1H), 4.38 (s, 2H), 3.04 (t, J = 6.7 Hz, 2H), 2.92 (s, 3H), 2.83 (t, J = 6.3 Hz, 2H), 1.90–1.85 (m, 2H), 1.80–1.74 (m, 2 H) (Figure S11 in the Supporting Information); HRMS (ESI): m/z calcd for $C_{21}H_{23}N_2O$ $[M+H]^+$: 319.1805; found: 319.1813 (Figure S12 in the Supporting Information).

3-((methyl(7-methyl-1,2,3,4-tetrahydroacridin-9-yl)amino)methyl)phenol (**4b**). Yield 80%; yellow solid; ^{1}H NMR (600 MHz, Chloroform-*d*) δ 8.11 (d, J = 8.6 Hz, 1H), 7.74 (s, 1H), 7.45 (dd, J = 8.6, 1.8 Hz, 1H), 7.12 (t, J = 7.8 Hz, 1H), 6.83 (dd, J = 8.0, 2.5 Hz, 1H), 6.77 (t, J = 2.0 Hz, 1H), 6.69 (d, J = 7.5 Hz, 1H), 4.44 (s, 2H), 3.22 (t, J = 6.6 Hz, 2H), 3.01 (s, 3H), 2.67 (t, J = 6.2 Hz, 2H), 2.49 (s, 3H), 1.84 (m, 2H), 1.77–1.69 (m, 2H) (Figure S13 in the Supporting Information); HRMS (ESI): m/z calcd for $C_{22}H_{25}N_2O$ $[M+H]^+$: 333.1961; found: 333.1991 (Figure S14 in the Supporting Information).

3-(((7-fluoro-1,2,3,4-tetrahydroacridin-9-yl)(methyl)amino)methyl)phenol (**4c**). Yield 72%; pale yellow solid; ^{1}H NMR (600 MHz, DMSO-d_6) δ 9.37 (s, 1H), 7.91 (dd, J = 9.2, 5.6 Hz, 1H), 7.70 (dd, J = 10.7, 2.9 Hz, 1H), 7.52 (td, J = 8.7, 2.8 Hz, 1H), 7.13 (t, J = 8.0 Hz, 1H), 6.76–6.70 (m, 2H), 6.68–6.63 (m, 1H), 4.27 (s, 2H), 2.99 (t, J = 6.7 Hz, 2H), 2.83 (s, 3H), 2.81 (d, J = 6.4 Hz, 2H), 1.85 (p, J = 6.4 Hz, 2H), 1.75 (p, J = 6.0 Hz, 2H) (Figure S15 in the Supporting Information); HRMS (ESI): m/z calcd for $C_{21}H_{22}FN_2O$ $[M+H]^+$: 337.1711; found: 337.1746 (Figure S16 in the Supporting Information).

(4-((methyl(1,2,3,4-tetrahydroacridin-9-yl)amino)methyl)phenyl)methanol (**4d**). Yield 69%; yellow solid; ^{1}H NMR (600 MHz, Methylene Chloride-d_2) δ 8.09 (dd, J = 8.5, 1.4 Hz, 1H), 7.89 (dt, J = 8.4, 0.9 Hz, 1H), 7.57 (ddd, J = 8.3, 6.8, 1.4 Hz, 1H), 7.43 (ddd, J = 8.2, 6.7, 1.3 Hz, 1H), 7.35–7.30 (m, 4H), 4.67 (s, 2H), 4.40 (s, 2H), 3.07 (t, J = 6.7 Hz, 2H), 2.90 (s, 3H), 2.86 (t, J = 6.4 Hz, 2H), 1.96–1.90 (m, 2H), 1.84–1.79 (m, 2H) (Figure S17 in the Supporting Information); HRMS (ESI): m/z calcd for $C_{22}H_{25}N_2O$ $[M+H]^+$: 333.1961; found: 333.2016 (Figure S18 in the Supporting Information).

(4-((methyl(7-methyl-1,2,3,4-tetrahydroacridin-9-yl)amino)methyl)phenyl)methanol (**4e**). Yield 76%; yellow solid; ^{1}H NMR (600 MHz, Chloroform-*d*) δ 8.36 (d, J = 8.6 Hz, 1H), 7.73 (s, 1H), 7.57–7.48 (m, 1H), 7.35 (d, J = 8.1 Hz, 2H), 7.20 (dd, J = 8.1, 2.8 Hz, 2H), 4.72 (d, J = 1.9 Hz, 2H), 4.52 (s, 2H), 3.37 (t, J = 6.6 Hz, 2H), 3.00 (d, J = 2.0 Hz, 3H), 2.77–2.67 (m, 2H), 2.51 (d, J = 2.2 Hz, 3H), 1.91 (dp, J = 10.3, 3.9 Hz, 2H), 1.78 (qd, J = 5.8, 2.4 Hz, 2H) (Figure

S19 in the Supporting Information); HRMS (ESI): m/z calcd for $C_{23}H_{27}N_2O$ $[M+H]^+$: 347.2118; found: 347.2170 (Figure S20 in the Supporting Information).

General Procedure for the Preparation of Compounds 6a-o and 7a-l

To a solution of compound **4a-4e** (3.10 mmol, 1.0 equiv.) in dry DMF (20mL), NaH (6.20 mmol, 2.0 equiv., 60% mineral oil) was added under the protection of nitrogen atmosphere and stirred at 0 °C for 30 min. Next, dibromide (18.6 mmol, 6.0 equiv.) was added and stirred at room temperature for 12 h. After completion, the reaction was quenched by ice water. The reaction mixture was extracted with EA (30 mL × 3), and the organic phase was washed with saturated salt water as well as dried with anhydrous Na_2SO_4. The crude product without excess solvent was purified by column chromatography (PE /EA: 4/1~1/1, v/v) to give compounds **5a-5e** as pale yellow or yellow oil.[33] A mixture of compound **5a-e** (2.32 mmol, 1.0 equiv.) and K_2CO_3 (11.60 mmol, 5.0 equiv.) in acetonitrile (23 mL), *N*-methylpropargylamine (4.64 mmol, 2.0 equiv.) was added. The reaction was stirred for 12 h at 70 °C, the solvent was removed by vacuum, and appropriate water was added and extracted with DCM (30 mL × 3). The combined organic phases were washed with saturated salt water, dried with anhydrous Na_2SO_4, filtered, and concentrated under a vacuum. The crude product was purified by silica gel chromatography (PE/EA: 1/1~1/3 to DCM/MeOH: 20/1~10/1, v/v) to get the target compounds **6a-6o** and **7a-7l**.[21]

N-methyl-*N*-(3-(2-(methyl(prop-2-yn-1-yl)amino)ethoxy)benzyl)-1,2,3,4-tetrahydroacridin-9-amine (**6a**). Yield 62%; pale yellow oil; ^{1}H NMR (600 MHz, Methylene Chloride-d_2) δ 8.08 (dd, J = 8.4, 1.4 Hz, 1H), 8.00 (d, J = 8.4 Hz, 1H), 7.60 (ddd, J = 8.3, 6.7, 1.4 Hz, 1H), 7.45 (ddd, J = 8.2, 6.7, 1.3 Hz, 1H), 7.24 (t, J = 7.8 Hz, 1H), 6.91 (d, J = 7.5 Hz, 1H), 6.87 (t, J = 2.1 Hz, 1H), 6.84–6.79 (m, 1H), 4.41 (s, 2H), 3.99 (t, J = 5.7 Hz, 2H), 3.41 (d, J = 2.4 Hz, 2H), 3.13 (t, J = 6.7 Hz, 2H), 2.95 (s, 3H), 2.85 (t, J = 6.3 Hz, 2H), 2.82 (t, J = 5.7 Hz, 2H), 2.37 (s, 3H), 2.28 (t, J = 2.4 Hz, 1H), 1.96–1.91 (m, 2H), 1.82 (ddt, J = 9.5, 6.2, 3.5 Hz, 2H) (Figure S21 in the Supporting Information). ^{13}C NMR (150 MHz, Chloroform-*d*) δ 160.59, 159.08, 154.51, 148.09, 141.12, 129.48, 128.98, 128.41, 127.96, 126.04, 125.01, 124.47, 121.19, 114.73, 113.65, 78.46, 73.53, 66.03, 60.43, 54.47, 46.10, 42.35, 40.50, 34.11, 27.03, 23.13, 23.03 (Figure S22 in the Supporting Information). HRMS (ESI): m/z calcd for $C_{27}H_{32}N_3O$ $[M+H]^+$: 414.2540; found: 414.2603 (Figure S23 in the Supporting Information).

N-methyl-*N*-(3-(3-(methyl(prop-2-yn-1-yl)amino)propoxy)benzyl)-1,2,3,4-tetrahydroacridin-9-amine (**6b**). Yield 57%; pale yellow oil; ^{1}H NMR (600 MHz, DMSO-d_6) δ 8.07 (d, J = 8.4 Hz, 1H), 7.85 (d, J = 8.3 Hz, 1H), 7.62–7.57 (m, 1H), 7.49–7.44 (m, 1H), 7.22 (t, J = 7.8 Hz, 1H), 6.89 (d, J = 7.5 Hz, 1H), 6.86 (s, 1H), 6.80 (dd, J = 8.2, 2.4 Hz, 1H), 4.36 (s, 2H), 3.92 (t, J = 6.4 Hz, 2H), 3.25 (d, J = 2.5 Hz, 2H), 3.07–3.03 (m, 1H), 3.00 (t, J = 6.7 Hz, 2H), 2.88 (s, 3H), 2.84 (t, J = 6.4 Hz, 2H), 2.46 (t, J = 7.1 Hz, 2H), 2.20 (s, 3H), 1.89–1.83 (m, 2H), 1.81 (q, J = 6.8 Hz, 2H), 1.76 (q, J = 6.2 Hz, 2H) (Figure S24 in the Supporting Information). ^{13}C NMR (150 MHz, DMSO-d_6) δ 159.83, 158.63, 153.33, 147.42, 140.81, 129.19, 128.57, 127.95, 127.64, 125.37, 124.73, 123.99, 120.39, 114.09, 113.40, 78.93, 75.40, 65.57, 59.28, 51.65, 44.95, 41.14, 40.20, 33.34, 26.69, 25.92, 22.36, 22.22 (Figure S25 in the Supporting Information). HRMS (ESI): m/z calcd for $C_{28}H_{34}N_3O$ $[M+H]^+$: 428.2696; found: 428.2763 (Figure S26 in the Supporting Information).

N-methyl-*N*-(3-(4-(methyl(prop-2-yn-1-yl)amino)butoxy)benzyl)-1,2,3,4-tetrahydroacridin-9-amine (**6c**). Yield 80%; pale yellow oil; ^{1}H NMR (600 MHz, DMSO-d_6) δ 8.08 (d, J = 8.4 Hz, 1H), 7.85 (d, J = 8.3 Hz, 1H), 7.60 (ddd, J = 8.3, 6.7, 1.4 Hz, 1H), 7.50–7.44 (m, 1H), 7.23 (t, J = 7.8 Hz, 1H), 6.89 (d, J = 7.5 Hz, 1H), 6.86 (t, J = 2.0 Hz, 1H), 6.81 (dd, J = 8.2, 2.5 Hz, 1H), 4.36 (s, 2H), 3.91 (t, J = 6.5 Hz, 2H), 3.27 (s, 2H), 3.04 (d, J = 2.4 Hz, 1H), 3.00 (t, J = 6.7 Hz, 2H), 2.88 (s, 3H), 2.84 (t, J = 6.3 Hz, 2H), 2.37 (t, J = 7.2 Hz, 2H), 2.19 (s, 3H), 1.87 (p, J = 6.6 Hz, 2H), 1.76 (p, J = 6.3 Hz, 2H), 1.71–1.65 (m, 2H), 1.50 (p, J = 7.3 Hz, 2H) (Figure S27 in the Supporting Information). ^{13}C NMR (150 MHz, DMSO-d_6) δ 162.86, 160.22, 158.93, 154.01, 147.09, 141.12, 129.69, 128.63, 127.93, 125.62, 125.29, 124.45, 120.73, 114.36, 113.70, 79.25, 75.99, 67.38, 59.56, 54.74, 45.07, 41.43, 40.59, 33.55, 26.68, 26.40, 23.58, 22.73, 22.54 (Figure S28 in the Supporting Information). HRMS (ESI): m/z calcd for $C_{29}H_{36}N_3O$ $[M+H]^+$: 442.2853; found: 442.2919 (Figure S29 in the Supporting Information).

N-methyl-*N*-(3-((5-(methyl(prop-2-yn-1-yl)amino)pentyl)oxy)benzyl)-1,2,3,4-tetrahydroacridin-9-amine (6d). Yield 86%; pale yellow oil; ^{1}H NMR (600 MHz, DMSO-d_6) δ 8.07 (d, J = 8.4 Hz, 1H), 7.85 (d, J = 8.3 Hz, 1H), 7.63–7.55 (m, 1H), 7.47 (dd, J = 8.4, 6.7 Hz, 1H), 7.22 (t, J = 8.0 Hz, 1H), 6.89 (d, J = 7.5 Hz, 1H), 6.85 (d, J = 2.4 Hz, 1H), 6.80 (dd, J = 8.2, 2.4 Hz, 1H), 4.36 (s, 2H), 3.88 (t, J = 6.6 Hz, 2H), 3.26 (s, 2H), 3.03 (t, J = 2.1 Hz, 1H), 3.00 (t, J = 6.7 Hz, 2H), 2.88 (d, J = 1.5 Hz, 3H), 2.84 (t, J = 6.4 Hz, 2H), 2.33 (t, J = 6.9 Hz, 2H), 2.18 (s, 3H), 1.86 (p, J = 6.8 Hz, 2H), 1.76 (p, J = 6.2 Hz, 2H), 1.67 (dp, J = 14.6, 7.1 Hz, 2H), 1.41 (dp, J = 22.3, 8.0 Hz, 4H) (Figure S30 in the Supporting

Information). ^{13}C NMR (150 MHz, DMSO-d_6) δ 159.84, 158.66, 153.33, 147.43, 140.78, 129.20, 128.58, 127.96, 127.67, 125.38, 124.72, 123.99, 120.34, 114.10, 113.38, 79.09, 75.27, 67.24, 59.28, 54.83, 44.88, 41.19, 40.22, 33.34, 28.41, 26.48, 25.92, 23.28, 22.37, 22.22 (Figure S31 in the Supporting Information). HRMS (ESI): m/z calcd for $C_{30}H_{38}N_3O$ $[M+H]^+$: 456.3009; found: 456.3077 (Figure S32 in the Supporting Information).

N-methyl-*N*-(3-((6-(methyl(prop-2-yn-1-yl)amino)hexyl)oxy)benzyl)-1,2,3,4-tetrahydroacridin-9-amine (**6e**). Yield 83%; pale yellow oil; ^{1}H NMR (600 MHz, DMSO-d_6) δ 8.07 (d, J = 8.4 Hz, 1H), 7.85 (d, J = 8.3 Hz, 1H), 7.60 (t, J = 7.6 Hz, 1H), 7.47 (t, J = 7.6 Hz, 1H), 7.22 (t, J = 7.8 Hz, 1H), 6.89 (d, J = 7.5 Hz, 1H), 6.85 (d, J = 2.6 Hz, 1H), 6.80 (dd, J = 8.2, 2.6 Hz, 1H), 4.36 (s, 2H), 3.88 (t, J = 6.5 Hz, 2H), 3.26 (d, J = 2.4 Hz, 2H), 3.03 (d, J = 2.4 Hz, 1H), 3.00 (t, J = 6.7 Hz, 2H), 2.88 (s, 3H), 2.84 (t, J = 6.4 Hz, 2H), 2.32 (t, J = 7.2 Hz, 2H), 2.17 (s, 3H), 1.86 (p, J = 6.5 Hz, 2H), 1.76 (p, J = 6.3 Hz, 2H), 1.66 (q, J = 6.9 Hz, 2H), 1.38 (tdd, J = 14.7, 9.4, 5.1 Hz, 4H), 1.30 (q, J = 7.7, 7.1 Hz, 2H) (Figure S33 in the Supporting Information). ^{13}C NMR (151 MHz, DMSO) δ 159.83, 158.66, 153.33, 147.42, 140.78, 129.19, 128.58, 127.95, 127.66, 125.38, 124.71, 123.99, 120.33, 114.06, 113.41, 79.07, 75.26, 67.22, 59.28, 54.85, 44.87, 41.19, 40.22, 33.34, 28.52, 26.75, 26.43, 25.92, 25.29, 22.37, 22.22 (Figure S34 in the Supporting Information). HRMS (ESI): m/z calcd for $C_{31}H_{40}N_3O$ $[M+H]^+$: 470.3166; found: 470.3234 (Figure S35 in the Supporting Information).

N-methyl-*N*-(3-((7-(methyl(prop-2-yn-1-yl)amino)heptyl)oxy)benzyl)-1,2,3,4-tetrahydroacridin-9-amine (**6f**). Yield 75%; pale yellow oil; ^{1}H NMR (600 MHz, DMSO-d_6) δ 8.07 (d, J = 8.4 Hz, 1H), 7.85 (d, J = 8.4 Hz, 1H), 7.60 (t, J = 7.5 Hz, 1H), 7.47 (t, J = 7.6 Hz, 1H), 7.22 (t, J = 7.8 Hz, 1H), 6.89 (d, J = 7.5 Hz, 1H), 6.84 (d, J = 2.4 Hz, 1H), 6.80 (dd, J = 8.2, 2.6 Hz, 1H), 4.36 (s, 2H), 3.88 (t, J = 6.6 Hz, 2H), 3.25 (d, J = 2.5 Hz, 2H), 3.02 (d, J = 2.4 Hz, 1H), 3.00 (t, J = 6.7 Hz, 2H), 2.88 (s, 3H), 2.84 (t, J = 6.4 Hz, 2H), 2.31 (t, J = 7.2 Hz, 2H), 2.16 (s, 3H), 1.86 (p, J = 6.6 Hz, 2H), 1.76 (q, J = 6.2 Hz, 2H), 1.66 (q, J = 7.0 Hz, 2H), 1.37 (dt, J = 10.6, 5.2 Hz, 4H), 1.32–1.26 (m, 4H) (Figure S36 in the Supporting Information). ^{13}C NMR (150 MHz, DMSO-d_6) δ 159.84, 158.67, 153.33, 147.43, 140.78, 129.19, 128.58, 127.95, 127.66, 125.38, 124.72, 124.00, 120.33, 114.07, 113.41, 79.09, 75.25, 67.23, 59.29, 54.90, 44.86, 41.19, 40.23, 40.06, 33.34, 28.48, 26.71, 26.66, 25.92, 25.36, 22.38, 22.23 (Figure S37 in the Supporting Information). HRMS (ESI): m/z calcd for $C_{32}H_{42}N_3O$ $[M+H]^+$: 484.3322; found: 484.3390 (Figure S38 in the Supporting Information).

N-methyl-*N*-(3-((8-(methyl(prop-2-yn-1-yl)amino)octyl)oxy)benzyl)-1,2,3,4-tetrahydroacridin-9-amine (**6g**). Yield 66%; pale yellow oil; ^{1}H NMR (600 MHz, DMSO-d_6) δ 8.08 (d, J = 8.4 Hz, 1H), 7.85 (dd, J = 8.4, 1.2 Hz, 1H), 7.60 (dd, J = 8.4, 6.8 Hz, 1H), 7.47 (dd, J = 8.4, 6.9 Hz, 1H), 7.22 (t, J = 7.8 Hz, 1H), 6.89 (d, J = 7.5 Hz, 1H), 6.85 (d, J = 2.6 Hz, 1H), 6.80 (dd, J = 8.2, 2.6 Hz, 1H), 4.36 (s, 2H), 3.88 (td, J = 6.6, 1.6 Hz, 2H), 3.25 (d, J = 2.4 Hz, 2H), 3.02 (t, J = 2.3 Hz, 1H), 3.00 (t, J = 6.7 Hz, 2H), 2.88 (s, 3H), 2.84 (t, J = 6.4 Hz, 2H), 2.31 (t, J = 7.3 Hz, 2H), 2.17 (s, 3H), 1.86 (p, J = 6.6 Hz, 2H), 1.76 (p, J = 6.3 Hz, 2H), 1.66 (q, J = 7.1 Hz, 2H), 1.41–1.35 (m, 4H), 1.32–1.25 (m, 6H) (Figure S39 in the Supporting Information). ^{13}C NMR (150 MHz, DMSO-d_6) δ 162.84, 160.19, 158.96, 153.98, 147.52, 141.09, 129.66, 128.57, 127.90, 125.61, 125.25, 124.43, 120.70, 114.23, 113.74, 79.18, 75.98, 67.49, 59.57, 55.16, 45.06, 41.50, 40.58, 33.56, 29.13, 28.94, 28.81, 26.99, 26.39, 25.72, 22.73, 22.54, 22.38 (Figure S40 in the Supporting Information). HRMS (ESI): m/z calcd for $C_{33}H_{44}N_3O$ $[M+H]^+$: 498.3479; found: 498.3546 (Figure S41 in the Supporting Information).

N,7-dimethyl-*N*-(3-(3-(methyl(prop-2-yn-1-yl)amino)propoxy)benzyl)-1,2,3,4-tetrahydroacridin-9-amine (**6h**). Yield 85%; yellow oil; ^{1}H NMR (600 MHz, Methylene Chloride-d_2) δ 7.88–7.85 (m, 1H), 7.80 (d, J = 8.5 Hz, 1H), 7.42 (dd, J = 8.5, 1.9 Hz, 1H), 7.23 (t, J = 7.8 Hz, 1H), 6.94–6.88 (m, 2H), 6.81 (ddd, J = 8.2, 2.6, 1.0 Hz, 1H), 4.36 (s, 2H), 3.95 (t, J = 6.4 Hz, 2H), 3.33 (d, J = 2.4 Hz, 2H), 3.05 (t, J = 6.7 Hz, 2H), 2.91 (s, 3H), 2.84 (t, J = 6.3 Hz, 2H), 2.56 (t, J = 7.1 Hz, 2H), 2.53 (s, 3H), 2.29 (s, 3H), 2.24 (t, J = 2.4 Hz, 1H), 1.94–1.87 (m, 4H), 1.83–1.78 (m, 2H) (Figure S42 in the Supporting Information). ^{13}C NMR (150 MHz, Chloroform-*d*) δ 159.28, 158.90, 154.83, 145.46, 140.85, 134.91, 131.03, 129.41, 127.80, 127.63, 125.69, 123.37, 120.87, 114.41, 113.73, 78.48, 73.28, 65.97, 60.47, 52.39, 45.72, 41.75, 40.49, 33.27, 27.48, 26.93, 22.99, 22.73, 22.12 (Figure S43 in the Supporting Information). HRMS (ESI): m/z calcd for $C_{29}H_{36}N_3O$ $[M+H]^+$: 442.2853; found: 442.2918 (Figure S44 in the Supporting Information).

N,7-dimethyl-*N*-(3-(4-(methyl(prop-2-yn-1-yl)amino)butoxy)benzyl)-1,2,3,4-tetrahydroacridin-9-amine (**6i**). Yield 86%; yellow oil; ^{1}H NMR (600 MHz, Methylene Chloride-d_2) δ 7.85 (d, J = 9.6 Hz, 2H), 7.43 (dd, J = 8.7, 1.9 Hz, 1H), 7.22 (q, J = 6.7, 5.7 Hz, 1H), 6.93–6.85 (m, 2H), 6.80 (dt, J = 9.4, 4.7 Hz, 1H), 4.38 (s, 2H), 3.91 (q, J = 6.7 Hz, 2H), 3.32 (d, J = 2.4 Hz, 2H), 3.07 (q, J = 6.6 Hz, 2H), 2.92 (s, 3H), 2.83 (q, J = 6.5 Hz, 2H), 2.53 (s, 3H), 2.47–2.38 (m, 2H), 2.27 (s, 3H), 2.24 (t, J = 2.4 Hz, 1H), 1.94–1.88 (m, 2H), 1.83–1.74 (m, 4H), 1.63–1.56 (m, 2H) (Figure S45 in the

Supporting Information). ^{13}C NMR (150 MHz, Chloroform-*d*) δ 159.53, 159.36, 153.89, 146.73, 141.25, 134.57, 130.54, 129.39, 128.81, 128.09, 126.02, 123.32, 120.92, 114.44, 113.72, 78.74, 73.14, 67.68, 60.44, 55.39, 45.66, 41.83, 40.39, 34.04, 27.26, 26.98, 24.29, 23.16, 23.08, 22.18 (Figure S46 in the Supporting Information). HRMS (ESI): m/z calcd for $C_{30}H_{38}N_3O[M+H]^+$: 456.3009; found: 456.3075 (Figure S47 in the Supporting Information).

N,7-dimethyl-*N*-(3-((5-(methyl(prop-2-yn-1-yl)amino)pentyl)oxy)benzyl)-1,2,3,4-tetrahydroacridin-9-amine (**6j**). Yield 87%; yellow oil; ^{1}H NMR (600 MHz, Methylene Chloride-d_2) δ 7.86 (s, 1H), 7.80 (d, *J* = 8.5 Hz, 1H), 7.42 (dd, *J* = 8.5, 1.9 Hz, 1H), 7.22 (t, *J* = 7.8 Hz, 1H), 6.94–6.87 (m, 2H), 6.80 (dd, *J* = 8.2, 2.6 Hz, 1H), 4.36 (s, 2H), 3.90 (t, *J* = 6.5 Hz, 2H), 3.31 (d, *J* = 2.4 Hz, 2H), 3.05 (t, *J* = 6.7 Hz, 2H), 2.91 (s, 3H), 2.84 (t, *J* = 6.3 Hz, 2H), 2.52 (s, 3H), 2.40 (t, *J* = 7.0 Hz, 2H), 2.26 (s, 3H), 2.24 (t, *J* = 2.4 Hz, 1H), 1.91 (d, *J* = 6.3 Hz, 2H), 1.82–1.75 (m, 4H), 1.53–1.43 (m, 4H) (Figure S48 in the Supporting Information). ^{13}C NMR (150 MHz, DMSO-d_6) δ 158.78, 158.26, 154.09, 144.87, 140.83, 134.45, 130.85, 130.30, 129.40, 127.36, 125.12, 123.21, 120.51, 113.94, 113.62, 77.17, 69.84, 67.16, 59.41, 54.67, 44.70, 40.77, 40.38, 32.72, 28.48, 26.17, 25.74, 23.24, 22.47, 22.19, 21.63 (Figure S49 in the Supporting Information). HRMS (ESI): m/z calcd for $C_{31}H_{40}N_3O$ $[M+H]^+$: 470.3166; found: 470.3232 (Figure S50 in the Supporting Information).

N,7-dimethyl-*N*-(3-((6-(methyl(prop-2-yn-1-yl)amino)hexyl)oxy)benzyl)-1,2,3,4-tetrahydroacridin-9-amine (**6k**). Yield 78%; yellow oil; ^{1}H NMR (600 MHz, Methylene Chloride-d_2) δ 7.86 (dt, *J* = 1.9, 0.9 Hz, 1H), 7.83 (d, *J* = 8.5 Hz, 1H), 7.43 (dd, *J* = 8.5, 2.0 Hz, 1H), 7.22 (d, *J* = 0.8 Hz, 1H), 6.91–6.87 (m, 2H), 6.80 (ddd, *J* = 8.2, 2.6, 1.0 Hz, 1H), 4.37 (s, 2H), 3.89 (t, *J* = 6.5 Hz, 2H), 3.31 (d, *J* = 2.4 Hz, 2H), 3.07 (t, *J* = 6.7 Hz, 2H), 2.91 (s, 3H), 2.84 (t, *J* = 6.3 Hz, 2H), 2.52 (s, 3H), 2.41–2.36 (m, 2H), 2.26 (s, 3H), 2.24 (t, *J* = 2.4 Hz, 1H), 1.91 (d, *J* = 6.4 Hz, 2H), 1.83–1.78 (m, 2H), 1.78–1.72 (m, 2H), 1.49–1.43 (m, 4H), 1.36 (d, *J* = 5.4 Hz, 2H) (Figure S51 in the Supporting Information). ^{13}C NMR (150 MHz, Chloroform-*d*) δ 159.40, 158.08, 156.30, 143.75, 140.35, 135.47, 131.81, 129.54, 127.03, 126.46, 125.30, 123.54, 120.75, 114.43, 113.79, 78.27, 73.46, 67.78, 60.64, 55.53, 45.50, 41.73, 40.74, 32.32, 29.76, 29.22, 27.25, 26.96, 23.99, 22.85, 22.32, 22.13 (Figure S52 in the Supporting Information). HRMS (ESI): m/z calcd for $C_{32}H_{42}N_3O$ $[M+H]^+$: 484.3322; found: 484.3386 (Figure S53 in the Supporting Information).

N,7-dimethyl-*N*-(3-((7-(methyl(prop-2-yn-1-yl)amino)heptyl)oxy)benzyl)-1,2,3,4-tetrahydroacridin-9-amine (**6L**). Yield 78%; yellow oil; ^{1}H NMR (600 MHz, Methylene Chloride-d_2) δ 7.89–7.85 (m, 1H), 7.78 (d, *J* = 8.5 Hz, 1H), 7.41 (dd, *J* = 8.5, 1.9 Hz, 1H), 7.22 (t, *J* = 7.7 Hz, 1H), 6.93–6.88 (m, 2H), 6.82–6.77 (m, 1H), 4.35 (s, 2H), 3.89 (t, *J* = 6.5 Hz, 2H), 3.30 (d, *J* = 2.4 Hz, 2H), 3.04 (t, *J* = 6.7 Hz, 2H), 2.90 (s, 3H), 2.85 (t, *J* = 6.4 Hz, 2H), 2.52 (s, 3H), 2.40–2.34 (m, 2H), 2.25 (s, 3H), 2.23 (t, *J* = 2.4 Hz, 1H), 1.94–1.89 (m, 2H), 1.84–1.71 (m, 6H), 1.48–1.40 (m, 4H), 1.35 (dt, *J* = 9.9, 6.5 Hz, 2H) (Figure S54 in the Supporting Information). ^{13}C NMR (150 MHz, Methylene Chloride-d_2) δ 159.83, 159.77, 153.90, 147.00, 141.73, 134.78, 130.52, 129.54, 128.98, 128.51, 126.30, 123.65, 121.03, 114.54, 113.93, 79.43, 72.81, 68.24, 60.59, 56.06, 45.84, 41.84, 40.49, 34.28, 29.69, 29.66, 27.90, 27.69, 27.21, 26.42, 23.44, 23.35, 22.11 (Figure S55 in the Supporting Information). HRMS (ESI): m/z calcd for $C_{33}H_{44}N_3O$ $[M+H]^+$: 498.3479; found: 498.3545 (Figure S56 in the Supporting Information).

N,7-dimethyl-*N*-(3-((8-(methyl(prop-2-yn-1-yl)amino)octyl)oxy)benzyl)-1,2,3,4-tetrahydroacridin-9-amine (**6m**). Yield 83%; yellow oil; ^{1}H NMR (600 MHz, Methylene Chloride-d_2) δ 7.87 (s, 1H), 7.78 (d, *J* = 8.5 Hz, 1H), 7.41 (dd, *J* = 8.6, 1.9 Hz, 1H), 7.22 (t, *J* = 7.8 Hz, 1H), 6.92–6.89 (m, 2H), 6.81–6.77 (m, 1H), 4.35 (s, 2H), 3.89 (t, *J* = 6.6 Hz, 2H), 3.30 (d, *J* = 2.4 Hz, 2H), 3.04 (t, *J* = 6.7 Hz, 2H), 2.90 (s, 3H), 2.85 (t, *J* = 6.3 Hz, 2H), 2.52 (s, 3H), 2.40–2.33 (m, 2H), 2.25 (s, 3H), 2.23 (t, *J* = 2.4 Hz, 1H), 1.94–1.88 (m, 2H), 1.81 (t, *J* = 6.1 Hz, 2H), 1.77–1.72 (m, 2H), 1.44 (dt, *J* = 10.9, 7.2 Hz, 4H), 1.37–1.30 (m, 6H) (Figure S57 in the Supporting Information). ^{13}C NMR (151 MHz, Methylene Chloride-d_2) δ 159.83, 159.78, 153.89, 147.01, 141.74, 134.78, 130.51, 129.54, 129.00, 128.51, 126.30, 123.65, 121.03, 114.54, 113.93, 79.45, 72.78, 68.26, 60.59, 56.09, 45.85, 41.84, 40.49, 34.30, 29.89, 29.76, 29.68, 27.96, 27.70, 27.21, 26.41, 23.45, 23.36, 22.11 (Figure S58 in the Supporting Information). HRMS (ESI): m/z calcd for $C_{34}H_{46}N_3O$ $[M+H]^+$: 512.3635; found: 512.3701 (Figure S59 in the Supporting Information).

7-fluoro-*N*-methyl-*N*-(3-((6-(methyl(prop-2-yn-1-yl)amino)hexyl)oxy)benzyl)-1,2,3,4-tetrahydroacridin-9-amine (**6n**). Yield 77%; yellow oil; ^{1}H NMR (600 MHz, Chloroform-*d*) δ 7.97 (dd, *J* = 9.2, 5.5 Hz, 1H), 7.70 (dd, *J* = 10.5, 2.8 Hz, 1H), 7.39–7.33 (m, 1H), 7.25–7.22 (m, 1H), 6.89 (d, *J* = 7.5 Hz, 1H), 6.85 (t, *J* = 2.0 Hz, 1H), 6.82 (dd, *J* = 8.2, 2.4 Hz, 1H), 4.33 (s, 2H), 3.90 (t, *J* = 6.5 Hz, 2H), 3.36 (d, *J* = 2.3 Hz, 2H), 3.11 (t, *J* = 6.7 Hz, 2H), 2.90 (s, 3H), 2.85 (t, *J* = 6.4 Hz, 2H), 2.43 (t, *J* = 7.5 Hz, 2H), 2.32 (s, 3H), 2.22 (d, *J* = 2.2 Hz, 1H), 1.96–1.92 (m, 2H), 1.81 (d, *J* = 12.6 Hz, 2H), 1.77 (q, *J* = 7.1 Hz, 2H), 1.49 (dt, *J* = 14.5, 7.2 Hz, 4H), 1.38 (q, *J* = 7.8, 7.4 Hz, 2H) (Figure S60 in the Supporting

Information). ^{13}C NMR (150 MHz, Chloroform-*d*) δ 160.01 (d, J_{C-F} = 243 Hz), 159.89 (d, J_{C-F} = 1.5 Hz), 159.43, 153.91 (d, J_{C-F} = 4.5 Hz), 145.15, 140.79, 131.33 (d, J_{C-F} = 9 Hz), 129.50, 128.87, 126.91 (d, J_{C-F} = 9 Hz), 120.81, 118.44 (d, J_{C-F} = 25.5 Hz), 115.88, 113.80, 107.81 (d, J_{C-F} = 22.5 Hz), 78.74, 73.12, 67.93, 60.20, 55.74, 45.62, 41.88, 40.18, 33.95, 29.36, 27.65, 27.30, 27.01, 26.13, 22.98, 22.94 (Figure S61 in the Supporting Information). HRMS (ESI): m/z calcd for $C_{31}H_{39}FN_3O$ $[M+H]^+$: 488.3072; found: 488.3133 (Figure S62 in the Supporting Information).

7-fluoro-*N*-methyl-*N*-(3-((8-(methyl(prop-2-yn-1-yl)amino)octyl)oxy)benzyl)-1,2,3,4-tetrahydroacridin-9-amine (**6o**). Yield 77%; yellow oil; ^{1}H NMR (600 MHz, Chloroform-*d*) δ 7.96 (dd, *J* = 9.2, 5.4 Hz, 1H), 7.70 (dd, *J* = 10.5, 2.8 Hz, 1H), 7.36 (td, *J* = 8.6, 2.8 Hz, 1H), 7.24 (t, *J* = 7.9 Hz, 1H), 6.88 (d, *J* = 7.5 Hz, 1H), 6.86 (d, *J* = 2.5 Hz, 1H), 6.82 (dd, *J* = 8.1, 2.5 Hz, 1H), 4.32 (s, 2H), 3.90 (t, *J* = 6.6 Hz, 2H), 3.34 (d, *J* = 2.5 Hz, 2H), 3.11 (t, *J* = 6.7 Hz, 2H), 2.90 (s, 3H), 2.84 (t, *J* = 6.4 Hz, 2H), 2.44–2.37 (m, 2H), 2.30 (s, 3H), 2.21 (t, *J* = 2.4 Hz, 1H), 1.94 (p, *J* = 6.5 Hz, 2H), 1.83–1.73 (m, 4H), 1.45 (q, *J* = 9.5 Hz, 4H), 1.34 (d, *J* = 9.7 Hz, 6H) (Figure S63 in the Supporting Information). ^{13}C NMR (150 MHz, Chloroform-*d*) δ 160.02 (d, J_{C-F} = 244.5 Hz), 159.9 (d, J_{C-F} = 3 Hz), 159.46, 153.91 (d, J_{C-F} = 6 Hz), 145.16, 140.78, 131.33 (d, J_{C-F} = 9 Hz), 129.50, 128.88, 126.92 (d, J_{C-F} = 9 Hz), 120.79, 118.44 (d, J_{C-F} = 25.5 Hz), 114.46, 113.80, 107.81 (d, J_{C-F} = 24 Hz), 78.78, 73.08, 68.02, 60.22, 55.86, 45.61, 41.89, 40.19, 33.96, 29.61, 29.44, 29.38, 27.71, 27.48, 27.01, 26.12, 22.98, 22.94 (Figure S64 in the Supporting Information). HRMS (ESI): m/z calcd for $C_{33}H_{43}FN_3O$ $[M+H]^+$: 516.3385; found: 516.3446 (Figure S65 in the Supporting Information).

N-methyl-*N*-(4-((3-(methyl(prop-2-yn-1-yl)amino)propoxy)methyl)benzyl)-1,2,3,4-tetrahydroacridin-9-amine (**7a**). Yield 37%; yellow oil; ^{1}H NMR (600 MHz, Methylene Chloride-d_2) δ 8.09 (dd, *J* = 8.4, 1.4 Hz, 1H), 7.89 (d, *J* = 8.4 Hz, 1H), 7.57 (ddd, *J* = 8.5, 6.8, 1.5 Hz, 1H), 7.43 (ddd, *J* = 8.2, 6.7, 1.3 Hz, 1H), 7.34–7.28 (m, 4H), 4.47 (s, 2H), 4.40 (s, 2H), 3.51 (t, *J* = 6.5 Hz, 2H), 3.31 (d, *J* = 2.4 Hz, 2H), 3.10–3.04 (m, 2H), 2.90 (s, 3H), 2.86 (t, *J* = 6.3 Hz, 2H), 2.50–2.46 (m, 2H), 2.27 (s, 3H), 2.24 (t, *J* = 2.4 Hz, 1H), 1.93 (p, *J* = 6.6 Hz, 2H), 1.84–1.79 (m, 2H), 1.77–1.73 (m, 2H) (Figure S66 in the Supporting Information). ^{13}C NMR (150 MHz, Chloroform-*d*) δ 158.20, 154.44, 150.89, 138.41, 137.20, 130.08, 129.52, 128.68, 128.17, 127.25, 126.47, 125.92, 125.04, 79.07, 72.72, 70.70, 68.60, 60.77, 52.69, 45.46, 41.47, 41.33, 32.06, 29.84, 27.38, 27.16, 22.67. HRMS (ESI): m/z calcd for $C_{29}H_{36}N_3O$ $[M+H]^+$: 442.2853; found: 442.2902 (Figure S67 in the Supporting Information).

N-methyl-*N*-(4-((4-(methyl(prop-2-yn-1-yl)amino)butoxy)methyl)benzyl)-1,2,3,4-tetrahydroacridin-9-amine (**7b**). Yield 89%; yellow oil; ^{1}H NMR (600 MHz, Methylene Chloride-d_2) δ 8.09 (dd, *J* = 8.3, 1.4 Hz, 1H), 7.89 (d, *J* = 8.4 Hz, 1H), 7.57 (ddd, *J* = 8.3, 6.7, 1.4 Hz, 1H), 7.43 (ddd, *J* = 8.1, 6.7, 1.3 Hz, 1H), 7.34–7.27 (m, 4H), 4.47 (s, 2H), 4.40 (s, 2H), 3.49 (t, *J* = 6.4 Hz, 2H), 3.30 (d, *J* = 2.4 Hz, 2H), 3.07 (t, *J* = 6.7 Hz, 2H), 2.90 (s, 3H), 2.86 (t, *J* = 6.3 Hz, 2H), 2.42–2.37 (m, 2H), 2.26 (s, 3H), 2.23 (t, *J* = 2.4 Hz, 1H), 1.93 (p, *J* = 6.6 Hz, 2H), 1.84–1.79 (m, 2H), 1.63–1.60 (m, 2H), 1.54–1.49 (m, 2H) (Figure S68 in the Supporting Information). ^{13}C NMR (150 MHz, Chloroform-*d*) δ 159.44, 157.88, 142.44, 138.46, 137.19, 131.09, 129.34, 128.66, 128.14, 126.41, 125.87, 125.03, 124.55, 74.84, 72.68, 70.68, 70.34, 60.74, 55.27, 45.20, 41.31, 32.04, 29.82, 27.50, 27.14, 23.76, 22.66, 21.67 (Figure S69 in the Supporting Information). HRMS (ESI): m/z calcd for $C_{30}H_{38}N_3O$ $[M+H]^+$: 456.3009; found: 456.3069 (Figure S70 in the Supporting Information).

N-methyl-*N*-(4-(((5-(methyl(prop-2-yn-1-yl)amino)pentyl)oxy)methyl)benzyl)-1,2,3,4-tetrahydroacridin-9-amine (**7c**). Yield 80%; yellow oil; ^{1}H NMR (600 MHz, Methylene Chloride-d_2) δ 8.11–8.08 (m, 1H), 7.89 (dd, *J* = 8.4, 1.3 Hz, 1H), 7.57 (ddd, *J* = 8.4, 6.8, 1.5 Hz, 1H), 7.43 (ddd, *J* = 8.2, 6.7, 1.3 Hz, 1H), 7.34–7.28 (m, 4H), 4.46 (s, 2H), 4.40 (s, 2H), 3.47 (t, *J* = 6.6 Hz, 2H), 3.30 (d, *J* = 2.4 Hz, 2H), 3.07 (t, *J* = 6.7 Hz, 2H), 2.90 (s, 3H), 2.86 (t, *J* = 6.3 Hz, 2H), 2.40–2.34 (m, 2H), 2.25 (s, 3H), 2.23 (t, *J* = 2.4 Hz, 1H), 1.93 (p, *J* = 6.6 Hz, 2H), 1.82 (ddt, *J* = 12.1, 9.1, 4.4 Hz, 2H), 1.63–1.61 (m, 2H), 1.45 (tt, *J* = 7.4, 5.9 Hz, 2H), 1.41–1.36 (m, 2H) (Figure S71 in the Supporting Information). ^{13}C NMR (150 MHz, Methylene Chloride-d_2) δ 160.95, 154.52, 148.41, 139.15, 138.33, 129.18, 128.96, 128.47, 128.36, 128.06, 126.38, 125.05, 124.81, 79.40, 72.96, 72.83, 70.86, 60.37, 55.98, 45.85, 41.84, 40.47, 34.40, 30.08, 27.77, 27.22, 24.40, 23.40, 23.30 (Figure S72 in the Supporting Information). HRMS (ESI): m/z calcd for $C_{31}H_{40}N_3O$ $[M+H]^+$: 470.3166; found: 470.3224 (Figure S73 in the Supporting Information).

N-methyl-*N*-(4-((((6-(methyl(prop-2-yn-1-yl)amino)hexyl)oxy)methyl)benzyl)-1,2,3,4-tetrahydroacridin-9-amine (**7d**). Yield 64%; yellow oil; ^{1}H NMR (600 MHz, Methylene Chloride-d_2) δ 8.09 (dd, *J* = 8.4, 1.4 Hz, 1H), 7.92–7.86 (m, 1H), 7.57 (ddd, *J* = 8.3, 6.7, 1.4 Hz, 1H), 7.43 (ddd, *J* = 8.2, 6.7, 1.3 Hz, 1H), 7.35–7.26 (m, 4H), 4.46 (s, 2H), 4.39 (s, 2H), 3.46 (t, *J* = 6.6 Hz, 2H), 3.29 (d, *J* = 2.4 Hz, 2H), 3.07 (t, *J* = 6.7 Hz, 2H), 2.90 (s, 3H), 2.86 (t, *J* = 6.3 Hz, 2H), 2.40–2.33 (m, 2H), 2.25 (s, 3H), 2.24–2.22 (m, 2H), 1.93 (p, *J* = 6.6 Hz, 2H), 1.82 (q, *J* = 6.1 Hz, 2H), 1.70–1.68 (m, 2H),

1.61–1.59 (m, 2H), 1.44–1.42 (m, 2H), 1.41–1.37 (m, 2H) (Figure S74 in the Supporting Information). ^{13}C NMR (150 MHz, Chloroform-*d*) δ 158.82, 157.25, 144.62, 138.10, 137.64, 129.82, 128.55, 127.88, 126.60, 126.15, 125.68, 125.02, 124.68, 74.04, 72.56, 70.57, 60.37, 55.44, 45.19, 41.42, 40.76, 32.70, 32.06, 29.64, 27.14, 26.92, 26.05, 25.65, 22.69, 22.07 (Figure S75 in the Supporting Information). HRMS (ESI): m/z calcd for $C_{32}H_{42}N_3O$ $[M+H]^+$: 484.3322; found: 484.3378 (Figure S76 in the Supporting Information).

N-methyl-*N*-(4-(((7-(methyl(prop-2-yn-1-yl)amino)heptyl)oxy)methyl)benzyl)-1,2,3,4-tetrahydroacridin-9-amine (**7e**). Yield 37%; yellow oil; ^{1}H NMR (600 MHz, Methylene Chloride-d_2) δ 8.11–8.07 (m, 1H), 7.89 (d, *J* = 8.4 Hz, 1H), 7.57 (ddd, *J* = 8.3, 6.7, 1.4 Hz, 1H), 7.43 (ddd, *J* = 8.3, 6.8, 1.3 Hz, 1H), 7.33–7.27 (m, 4H), 4.46 (s, 2H), 4.39 (s, 2H), 3.46 (t, *J* = 6.6 Hz, 2H), 3.29 (d, *J* = 2.4 Hz, 2H), 3.07 (t, *J* = 6.7 Hz, 2H), 2.90 (s, 3H), 2.86 (t, *J* = 6.3 Hz, 2H), 2.36 (dd, *J* = 8.2, 6.7 Hz, 2H), 2.24 (s, 3H), 2.22 (t, *J* = 2.4 Hz, 1H), 1.93 (p, *J* = 6.5 Hz, 2H), 1.82 (q, *J* = 6.1 Hz, 2H), 1.62–1.58 (m, 6H), 1.44–1.41 (m, 2H), 1.32–1.30 (m, 2H) (Figure S77 in the Supporting Information). ^{13}C NMR (150 MHz, Chloroform-*d*) δ 159.47, 154.42, 146.56, 138.17, 137.69, 128.64, 128.36, 128.24, 127.57, 127.36, 126.58, 125.17, 124.36, 77.48, 71.66, 69.62, 62.74, 59.22, 54.70, 44.60, 40.62, 40.31, 32.99, 29.20, 28.65, 26.55, 26.17, 25.69, 22.46, 22.19, 22.18 (Figure S78 in the Supporting Information). HRMS (ESI): m/z calcd for $C_{33}H_{44}N_3O$ $[M+H]^+$: 498.3479; found: 498.3526 (Figure S79 in the Supporting Information).

N-methyl-*N*-(4-(((8-(methyl(prop-2-yn-1-yl)amino)octyl)oxy)methyl)benzyl)-1,2,3,4-tetrahydroacridin-9-amine (**7f**). Yield 51%; yellow oil; ^{1}H NMR (600 MHz, Methylene Chloride-d_2) δ 8.09 (dd, *J* = 8.5, 1.4 Hz, 1H), 7.89 (dd, *J* = 8.5, 1.3 Hz, 1H), 7.57 (ddd, *J* = 8.4, 6.7, 1.5 Hz, 1H), 7.43 (ddd, *J* = 8.2, 6.7, 1.3 Hz, 1H), 7.34–7.27 (m, 4H), 4.46 (s, 2H), 4.39 (s, 2H), 3.46 (t, *J* = 6.6 Hz, 2H), 3.29 (d, *J* = 2.5 Hz, 2H), 3.07 (t, *J* = 6.7 Hz, 2H), 2.90 (s, 3H), 2.86 (t, *J* = 6.4 Hz, 2H), 2.39–2.32 (m, 2H), 2.24 (s, 3H), 2.22 (t, *J* = 2.4 Hz, 1H), 1.93 (p, *J* = 6.6 Hz, 2H), 1.85–1.78 (m, 2H), 1.73–1.65 (m, 4H), 1.62–1.57 (m, 2H), 1.45–1.39 (m, 2H), 1.39–1.32 (m, 4H) (Figure S80 in the Supporting Information). ^{13}C NMR (150 MHz, Chloroform-*d*) δ 160.14, 155.39, 147.12, 138.48, 137.95, 128.81, 128.75, 128.27, 127.93, 127.63, 125.80, 125.23, 124.55, 78.51, 73.31, 72.78, 70.80, 60.31, 55.82, 45.54, 41.82, 40.48, 29.88, 29.83, 29.61, 29.55, 27.60, 27.48, 27.02, 26.29, 23.04, 22.81 (Figure S81 in the Supporting Information). HRMS (ESI): m/z calcd for $C_{34}H_{46}N_3O$ $[M+H]^+$: 512.3635; found: 512.3688 (Figure S82 in the Supporting Information).

N,7-dimethyl-*N*-(4-((3-(methyl(prop-2-yn-1-yl)amino)propoxy)methyl)benzyl)-1,2,3,4-tetrahydroacridin-9-amine (**7g**). Yield 29%; pale yellow oil; ^{1}H NMR (600 MHz, Chloroform-*d*) δ 8.01 (d, *J* = 8.6 Hz, 1H), 7.79 (s, 1H), 7.46 (d, *J* = 8.5 Hz, 1H), 7.32 (d, *J* = 7.8 Hz, 2H), 7.28 (d, *J* = 7.9 Hz, 2H), 4.51 (s, 2H), 4.42 (s, 2H), 3.55 (t, *J* = 6.5 Hz, 2H), 3.36 (d, *J* = 2.9 Hz, 2H), 3.19 (t, *J* = 6.7 Hz, 2H), 2.92 (s, 3H), 2.80 (t, *J* = 6.3 Hz, 2H), 2.55 (t, *J* = 7.4 Hz, 2H), 2.53 (s, 3H), 2.32 (s, 3H), 2.22 (q, *J* = 2.0 Hz, 1H), 1.92 (q, *J* = 6.7, 6.2 Hz, 2H), 1.84–1.77 (m, 4H) (Figure S83 in the Supporting Information). ^{13}C NMR (150 MHz, Chloroform-*d*) δ 158.72, 157.73, 145.05, 138.46, 137.82, 135.21, 131.37, 128.77, 127.95, 127.92, 127.51, 125.60, 123.43, 78.54, 73.34, 72.84, 68.80, 60.36, 52.74, 45.71, 41.80, 40.52, 29.84, 27.94, 26.99, 23.00, 22.66, 22.21. HRMS (ESI): m/z calcd for $C_{30}H_{38}N_3O$ $[M+H]^+$: 456.3009; found: 456.3047 (Figure S84 in the Supporting Information).

N,7-dimethyl-*N*-(4-((4-(methyl(prop-2-yn-1-yl)amino)butoxy)methyl)benzyl)-1,2,3,4-tetrahydroacridin-9-amine (**7h**). Yield 42%; pale yellow oil; ^{1}H NMR (600 MHz, Chloroform-*d*) δ 8.11 (d, *J* = 8.7 Hz, 1H), 7.79 (s, 1H), 7.49 (dd, *J* = 8.7, 1.9 Hz, 1H), 7.32 (d, *J* = 7.8 Hz, 2H), 7.27 (d, *J* = 5.1 Hz, 2H), 4.51 (s, 2H), 4.45 (s, 2H), 3.52 (t, *J* = 6.4 Hz, 2H), 3.36 (d, *J* = 2.4 Hz, 2H), 3.24 (t, *J* = 6.7 Hz, 2H), 2.95 (s, 3H), 2.79 (t, *J* = 6.3 Hz, 2H), 2.53 (s, 3H), 2.50–2.45 (m, 2H), 2.33 (s, 3H), 2.22 (t, *J* = 2.4 Hz, 1H), 1.93 (dt, *J* = 13.1, 6.7 Hz, 2H), 1.80 (p, *J* = 6.2 Hz, 2H), 1.69–1.64 (m, 2H), 1.61–1.56 (m, 2H) (Figure S85 in the Supporting Information). ^{13}C NMR (150 MHz, Chloroform-*d*) δ 159.09, 156.22, 144.03, 138.12, 138.07, 135.56, 131.86, 128.74, 127.96, 127.14, 126.58, 125.38, 123.52, 78.40, 73.42, 72.75, 70.48, 60.48, 55.53, 45.56, 41.75, 40.69, 29.83, 27.65, 27.00, 24.32, 22.91, 22.40, 22.20 (Figure S86 in the Supporting Information). HRMS (ESI): m/z calcd for $C_{31}H_{40}N_3O$ $[M+H]^+$: 470.3166; found: 470.3222 (Figure S87 in the Supporting Information).

N,7-dimethyl-*N*-(4-(((5-(methyl(prop-2-yn-1-yl)amino)pentyl)oxy)methyl)benzyl)-1,2,3,4-tetrahydroacridin-9-amine (**7i**). Yield 61%; pale yellow oil; ^{1}H NMR (600 MHz, Chloroform-*d*) δ 7.92 (d, *J* = 8.5 Hz, 1H), 7.80 (s, 1H), 7.42 (dd, *J* = 8.5, 1.9 Hz, 1H), 7.33–7.26 (m, 4H), 4.49 (s, 2H), 4.38 (s, 2H), 3.48 (t, *J* = 6.6 Hz, 2H), 3.33 (d, *J* = 2.4 Hz, 2H), 3.13 (t, *J* = 6.7 Hz, 2H), 2.89 (s, 3H), 2.80 (t, *J* = 6.4 Hz, 2H), 2.51 (s, 3H), 2.44–2.38 (m, 2H), 2.29 (s, 3H), 2.20 (t, *J* = 2.4 Hz, 1H), 1.92 (p, *J* = 6.5 Hz, 2H), 1.79 (p, *J* = 6.2 Hz, 2H), 1.65 (p, *J* = 6.8 Hz, 2H), 1.48 (p, *J* = 7.2 Hz, 2H), 1.44–1.36 (m, 2H) (Figure S88 in the Supporting Information). ^{13}C NMR (150 MHz, Chloroform-*d*) δ 159.14, 154.42, 146.00, 138.64, 137.73, 134.77, 130.80, 128.74, 128.21, 127.85, 127.83, 125.81, 123.29, 78.61, 73.16, 72.81, 70.56, 60.22, 55.67, 45.55, 41.83, 40.33, 33.59, 29.73, 27.46, 26.91, 24.12,

23.04, 22.86, 22.14 (Figure S89 in the Supporting Information). HRMS (ESI): m/z calcd for $C_{32}H_{42}N_3O$ $[M+H]^+$: 484.3322; found: 484.3375 (Figure S90 in the Supporting Information).

N,7-dimethyl-*N*-(4-(((6-(methyl(prop-2-yn-1-yl)amino)hexyl)oxy)methyl)benzyl)-1,2,3,4-tetrahydroacridin-9-amine (**7j**). Yield 82%; pale yellow oil; ^{1}H NMR (600 MHz, Chloroform-*d*) δ 8.01 (d, *J* = 8.6 Hz, 1H), 7.78 (s, 1H), 7.45 (dd, *J* = 8.6, 1.9 Hz, 1H), 7.33–7.25 (m, 4H), 4.49 (s, 2H), 4.41 (s, 2H), 3.48 (t, *J* = 6.7 Hz, 2H), 3.34 (d, *J* = 2.4 Hz, 2H), 3.18 (t, *J* = 6.7 Hz, 2H), 2.92 (s, 3H), 2.79 (t, *J* = 6.4 Hz, 2H), 2.52 (s, 3H), 2.43–2.38 (m, 2H), 2.30 (s, 3H), 2.20 (t, *J* = 2.4 Hz, 1H), 1.92 (p, *J* = 6.6 Hz, 2H), 1.79 (p, *J* = 6.0 Hz, 2H), 1.63 (p, *J* = 6.8 Hz, 2H), 1.46 (p, *J* = 7.5 Hz, 2H), 1.39 (p, *J* = 7.0 Hz, 2H), 1.33 (q, *J* = 8.4, 7.8 Hz, 2H) (Figure S91 in the Supporting Information). ^{13}C NMR (150 MHz, Chloroform-*d*) δ 158.63, 155.33, 144.93, 138.34, 137.92, 135.14, 131.31, 128.72, 127.92, 127.89, 127.43, 125.54, 123.40, 78.47, 73.28, 72.74, 70.67, 60.33, 55.71, 45.52, 41.80, 40.49, 33.02, 29.80, 27.56, 27.35, 26.94, 26.24, 22.96, 22.61, 22.16 (Figure S92 in the Supporting Information). HRMS (ESI): m/z calcd for $C_{33}H_{44}N_3O$ $[M+H]^+$: 498.3479; found: 498.3529 (Figure S93 in the Supporting Information).

N,7-dimethyl-*N*-(4-(((7-(methyl(prop-2-yn-1-yl)amino)heptyl)oxy)methyl)benzyl)-1,2,3,4-tetrahydroacridin-9-amine (**7k**). Yield 61%; pale yellow oil; ^{1}H NMR (600 MHz, Chloroform-*d*) δ 8.31 (d, *J* = 8.6 Hz, 1H), 7.75 (s, 1H), 7.53 (d, *J* = 8.6 Hz, 1H), 7.32 (d, *J* = 7.7 Hz, 2H), 7.22 (d, *J* = 7.6 Hz, 2H), 4.50 (s, 2H), 4.49 (s, 2H), 3.51–3.45 (m, 2H), 3.42 (d, *J* = 2.5 Hz, 2H), 3.35 (t, *J* = 6.7 Hz, 2H), 2.99 (s, 3H), 2.74 (t, *J* = 6.3 Hz, 2H), 2.52 (s, 3H), 2.49 (t, *J* = 7.7 Hz, 2H), 2.37 (s, 3H), 2.27 (t, *J* = 2.4 Hz, 1H), 1.92 (p, *J* = 6.6 Hz, 2H), 1.79 (p, *J* = 6.0 Hz, 2H), 1.62 (p, *J* = 6.7 Hz, 2H), 1.50 (q, *J* = 7.0, 6.5 Hz, 2H), 1.38–1.31 (m, 6H) (Figure S94 in the Supporting Information). ^{13}C NMR (150 MHz, Chloroform-*d*) δ 157.93, 156.65, 143.34, 138.22, 137.91, 135.73, 132.12, 128.72, 127.98, 126.95, 126.10, 125.25, 123.57, 77.80, 73.89, 72.72, 70.81, 60.52, 55.60, 45.29, 41.54, 40.75, 32.03, 29.81, 29.46, 27.42, 27.20, 27.00, 26.25, 22.84, 22.25, 22.19 (Figure S95 in the Supporting Information). HRMS (ESI): m/z calcd for $C_{34}H_{46}N_3O$ $[M+H]^+$: 512.3635; found: 512.3678 (Figure S96 in the Supporting Information).

N,7-dimethyl-*N*-(4-(((8-(methyl(prop-2-yn-1-yl)amino)octyl)oxy)methyl)benzyl)-1,2,3,4-tetrahydroacridin-9-amine (**7l**). Yield 65%; pale yellow oil; ^{1}H NMR (600 MHz, Chloroform-*d*) δ 8.03 (s, 1H), 7.79 (s, 1H), 7.51–7.41 (m, 1H), 7.32 (d, *J* = 8.0 Hz, 2H), 7.28 (d, *J* = 7.9 Hz, 2H), 4.50 (s, 2H), 4.42 (s, 2H), 3.48 (t, *J* = 6.7 Hz, 2H), 3.35 (d, *J* = 2.4 Hz, 2H), 3.20 (s, 2H), 2.93 (s, 3H), 2.80 (t, *J* = 6.3 Hz, 2H), 2.53 (s, 3H), 2.45–2.38 (m, 2H), 2.31 (s, 3H), 2.22 (t, *J* = 2.4 Hz, 1H), 1.93 (p, *J* = 6.6 Hz, 2H), 1.82–1.77 (m, 2H), 1.62 (p, *J* = 6.8 Hz, 2H), 1.46 (q, *J* = 7.5 Hz, 2H), 1.37 (t, *J* = 7.3 Hz, 2H), 1.34–1.30 (m, 6H) (Figure S97 in the Supporting Information). ^{13}C NMR (150 MHz, Chloroform-*d*) δ 158.05, 156.59, 143.62, 138.19, 137.97, 135.64, 131.99, 128.72, 127.97, 127.03, 126.32, 125.31, 123.55, 77.89, 73.81, 72.72, 70.85, 60.49, 55.65, 45.32, 41.58, 40.71, 32.19, 29.85, 29.55, 29.51, 27.42, 27.28, 26.99, 26.26, 22.86, 22.31, 22.19 (Figure S98 in the Supporting Information). HRMS (ESI): m/z calcd for $C_{35}H_{48}N_3O$ $[M+H]^+$: 526.3792; found: 526.3851 (Figure S99 in the Supporting Information).

In vitro Inhibition Experiments of AChE/BuChE

To assess the inhibitory activity of compounds against AChE or BuChE, we followed the Ellman spectrophotometry method.[34] AChE (E.C. 3.1.1.7, *ee*AChE and human recombinant AChE from electric eel and human serum, respectively), BuChE (E.C. 3.1.1.8, *eq*BuChE and human recombinant BuChE from equine serum and human serum, respectively), 5.5 -dithiobis-(2-nitrobenzoic acid) (Ellman Reagent, DTNB), S-butylthiocholine iodide (BTCI), acetylthiocholine iodide (ATCI), and donepezil were obtained from Sigma-Aldrich. The tested compound was first dissolved in DMSO and then diluted with Tris-HCl buffer (pH = 8.0) to the required concentration (DMSO < 1%). Subsequently, 160 μL DTNB (1.5 mM), 50 μL AChE (0.25 U/mL *ee*AChE or *h*AChE) or 50 μL BuChE (0.12 U/mL *eq*BuChE or *h*BuChE), and 10 μL of test drug were successively added into the 96-well plate and incubated for 6 min at 37 °C. Then, 30 μL of the substrate (initial concentration of 3 mM, ATCI or BTCI) was added, and the absorbance values of 0, 60, 120, and 180 s were detected at 405nm in a microplate reader (SpectraMax Plus 384, Molecular Devices, CA, USA). The percent inhibition due to the presence of test compounds was calculated by the following expression: [1-(absorbance change of the experimental group/absorbance change of the blank group)] × 100%, where the absorbance changes in the experimental and blank groups were obtained in the presence and absence of the inhibitor, respectively. The concentration of the compound at 50% inhibition was calculated by Prism software (GraphPad, United States), and this value was considered as the IC_{50} of the compound. Each experiment was repeated three times, and the experimental results are expressed as mean ± SD.

In vitro Inhibition Experiments of hMAO-A and hMAO-B

The inhibitory effects of all synthetic compounds on MAOs were determined using an Amplex Red fluorescence assay with rasagiline and iproniazid as control drugs.[35] Human recombinant Monoamine oxidases (EC 1.4.3.4, *h*MAO-A and *h*MAO-B), Amplex Red reagent, horseradish peroxidase (HRP), rasagiline, and iproniazid were purchased from Sigma-Aldrich. The detailed experimental steps were as follows. The test compounds were dissolved in DMSO and diluted with PBS buffers (0.05 M, pH = 7.4) to prepare different final concentrations (DMSO < 1%). Various concentrations of test compounds (20 μL) were incubated with PBS buffer (80 μL) of *h*MAO-A or *h*MAO-B for 15 min at 37 °C in the dark. Next, the reaction was initiated by adding 100 μL of a mixture containing 200 μM of Amplex Red reagent, 2 U/mL of HRP, and 2 mM of tyramine (final concentration 1mM) to the system. The fluorescence changes of each solution within 20 min were recorded by a multi-detection microplate fluorescence reader (SpectraMax Plus 384, Molecular Devices, CA, USA). The detection conditions were an excitation wavelength of 545 nm and an emission wavelength of 590 nm. The percent inhibition due to the presence of test compounds was calculated by the following expression: [1-(change of fluorescence value of the experimental group/change of fluorescence value of the blank group)] × 100%, where the changes in fluorescence values of the experimental and blank groups were obtained in the presence and absence of the inhibitor, respectively. The concentration of the compound at 50% inhibition was calculated by Prism software (GraphPad, United States), and this value was considered as the IC_{50} of the compound. Experimental results are expressed as the mean ± SD of three independent experiments.

Docking Studies

Molecular simulations were performed using the Molecular Operating Environment (MOE) 2015.10 software (Chemical Computing Group, Montreal, Canada), following previously reported method.[36] The X-ray crystal structures of *h*AChE, *h*BuChE and *h*MAO-B (PDB codes: 4EY7, 7QHD and 2V61, respectively) downloaded from the Protein Data Bank (PDB) were processed by removing water molecules and adding charges. Compound **7d** was constructed through MOE's structure preparation module and subjected to energy minimization by the Merck Molecular force field (MMFF94x, RMSD gradient: 0.05 kcal mol^{-1} $Å^{-1}$), followed by docking to the active site of the corresponding protein via the Triangle Matcher method. Scoring and refinement were performed using the ASE scoring function and Force field, respectively. From the output, the optimal 10 conformations were retained. Finally, MOE's pose viewer utility was employed to analyze the geometry of the docking complex.

PAMPA-BBB Penetration Assay

Based on the previous work of Di et al, parallel artificial membrane permeation analysis (PAMPA) with the blood-brain barrier was used to predict the brain permeation capacity of the tested compounds.[37] Commercially available drugs, as well as DMSO and dodecane, were purchased from Sigma and Aladdin, while porcine brain phospholipids (PBL) were provided by Avanti Polar Lipids. Donor 96-well filter plates (PVDF membrane, pore size 0.45 μM) and acceptor indented 96-well microplates were obtained from Corning Inc., the 96-well UV plate was sourced from Millipore. The commercially available drug and the tested compound were dissolved in DMSO and diluted with PBS/EtOH (70/30, v/v) buffer to achieve a concentration of 25 μg/mL in the tested well. A 20 mg/mL dodecane solution of 4 μL PBL was evenly coated on the lipophilic filter membrane of the upper layer of a 96-well filter plate and left to stand for 5 min. Subsequently, 200 μL diluted solution of the tested drug and 300 μL PBS/EtOH (70/30, v/v) buffer were added to the donor and acceptor wells, respectively. The 96-well filter plate was placed over the acceptor plate to form a "sandwich" assembly, ensuring that the filter membrane could contact the buffer solution. Following incubation at 25 °C for 18 h, the donor plate was carefully removed, and the drug concentration was calculated by measuring the absorbance of the test compound in the donor, acceptor, and reference wells with a UV plate reader (SpectraMax Plus 384, Molecular Devices, CA, USA). Each sample was analyzed at five wavelengths, in four wells, and in at least three independent runs. The results are expressed as the means ± SD.

Cell Culture and Toxicity

For cell treatment, PC12 and BV-2 cells provided by the Stem Cell Bank of the Chinese Academy of Sciences were seeded in DMEM high glucose medium containing 10% fetal bovine serum, 100 U/mL penicillin, and 100 μg/mL streptomycin, and cultured under a humidified atmosphere with 5% CO_2 in air at 37 °C.

For cytotoxicity experiments, the CCK-8 assay was performed with donepezil as the reference compound.[38] The cells were planted in 96-well plates at a density of 10,000 per well and incubated in 1% fetal bovine serum medium for 24 h with six concentrations of compound **7d** or donepezil (0.3125, 0.625, 1.25, 2.5, 5, and 10 μM) after the cell growth met the requirements. After the incubation period, we removed the medium and added 100 μL of medium containing 10% CCK-8 to each well in the dark and incubated for 4 h, and the absorbance was detected at 450 nm to calculate the cell viability.

In vivo Acute Toxicity

After 5 days of adaptive feeding under standard conditions, 40 Kunming mice (20–24 g, half male and half female) were randomly divided into four groups: control group, high-, medium-, and low-dose groups (2500 mg/kg, 1250 mg/kg, and 625 mg/kg, respectively), with 10 mice in each group.[36,38,39] Compound **7d** was uniformly dispersed in 0.5% sodium carboxymethyl cellulose (CMC-Na) salt solution and administered orally according to the divided groups. The mice were closely monitored for death, dietary and behavioral abnormalities within 4 h after administration, and were then observed for 14 days and recorded in detail. On the 14th day after administration, all the mice were sacrificed after being anesthetized with ether. The heart, liver, kidney, lung and brain tissues of the high-dose and control mice were collected, and the tissues' pathological damage was observed by HE staining.

In vivo Step-Down Passive Avoidance Test

Scopolamine hydrobromide injection and donepezil hydrochloride were obtained from Zhengzhou Suicheng Pharmaceutical Co., Ltd and Annaiji Chemical Co., Ltd, respectively. Clean-grade male Kunming mice (18–22 g) from Hunan SJA Laboratory Animal Co., Ltd were housed under standard control conditions (22 ± 2 °C, 55 ± 10% humidity, 12 h: 12 h light:dark cycle) with free access to water and food. The step-down test, consisting of a training trial and a recall trial, was performed in a passive avoidance chamber with a steel grated floor and a plastic platform in the bottom right corner.[38,40,41]

During the training trial, each mouse was allowed to acclimatize to the chamber's environment for 5 min before the power supply was turned on and the current stimulation intensity was set to 0.5 mA (24 V). When the mice stepped down onto the steel grated floor, they received an electric shock that prompted them to return to the platform to avoid injury from the stimulus. For the passive avoidance test, 48 mice were randomly divided into 6 groups with 8 mice in each group. Compound **7d** and donepezil were suspended in a 0.5% CMC-Na solution to prepare the required concentrations. One hour before the training trial, the mice were given oral doses of compound **7d** (20, 10 and 5 mg/kg) or donepezil (10 mg/kg, positive control). After 30 min, mice were injected with scopolamine hydrobromide (3 mg/kg) intraperitoneally to induce memory impairment.[40,41] The recall trial was conducted 24 hours after training. During this trial, the mice were placed once again on the platform, and the latency to step down onto the grid for the first time and errors that caused an electric shock within 5 min were recorded. Latency and the number of errors were used to evaluate learning and memory performance.

Pharmacokinetics Assay in Sprague-Dawley Rats

The pharmacokinetic parameters of compound **7d** were determined in male SD rats (n = 3, 220 ± 20 g).[42,43] Samples were collected at appropriate time points (0.033, 0.083, 0.25, 0.5, 1, 2, 4, 6, 8, and 24 h) after administering **7d** to the rats by intravenous (1 mg/kg) or intraperitoneal (10 mg/kg) injection, followed by centrifugation at 10,000 rpm for 2 min and storage at −20 °C. Plasma proteins were precipitated with 0.5% formic acid/acetonitrile (v/v), and the supernatants obtained by centrifugation (14,000 rpm, 14 min) were analyzed using LC-MS/MS (Waters, ACQUITY-TQ-XS). The PK parameters were calculated by DAS2.0 software (China).

Statistical Analysis

The sample size of the step-down passive avoidance test was determined using Power Analysis and Sample Size (PASS) 15 software based on previous studies.[38,44] A two-sided significance level (α) of 0.05 and statistical power of 90% were selected, with equal group allocation ratios. By calculation, a minimum total of 48 mice should be included in the experiment. Thus, we included a total of 48 mice in this experiment, with 8 mice in each group. All data were tested for normality using Q-Q plots. For normally distributed data, the Brown-Forsythe test was used for homogeneity of variance, and results are presented as mean ± standard error of mean (SEM) (n = 8 per group). Statistical differences between groups were assessed using one-way analysis of variance (ANOVA) followed by Tukey's Multiple Comparison Test for

data with homogeneous variance. In cases where data did not meet the normal distribution, differences were evaluated using a Kruskal–Wallis test followed by Dunn's Multiple Comparison Test, and the results are expressed as boxplots, illustrating medians within boxes from the first quartile (25th percentile) to the third quartile (75th percentile) and whiskers ranging from minimum to maximum (n = 8 per group). A *p*-value of less than 0.05 was considered to indicate statistically significant differences with a 95% confidence interval (CI). Statistical analyses were performed using Prism software (GraphPad, United States).

Results

Chemistry

The target compounds were synthesized according to the procedure shown in Scheme 1. The initial compounds **1a-1c** and **2a-2b** were commercially available. Firstly, compounds **1a-1c** were reacted with the corresponding benzylamines **2a-2b** to obtain intermediates **3a-3e** in the presence of KI,[31] then a selective *N*-methylation was employed to afford compounds **4a-4e** with high yield by treatment with formaldehyde/acetic acid and the reductant $NaBH_3CN$,[32] followed by *O*-alkylation with the corresponding dibromide under NaH and DMF conditions to yield the key intermediates **5a-5e**.[33] Finally, the target compounds **6a-6o** and **7a-7l** were obtained via another *N*-alkylation of compounds **5a-5e** with

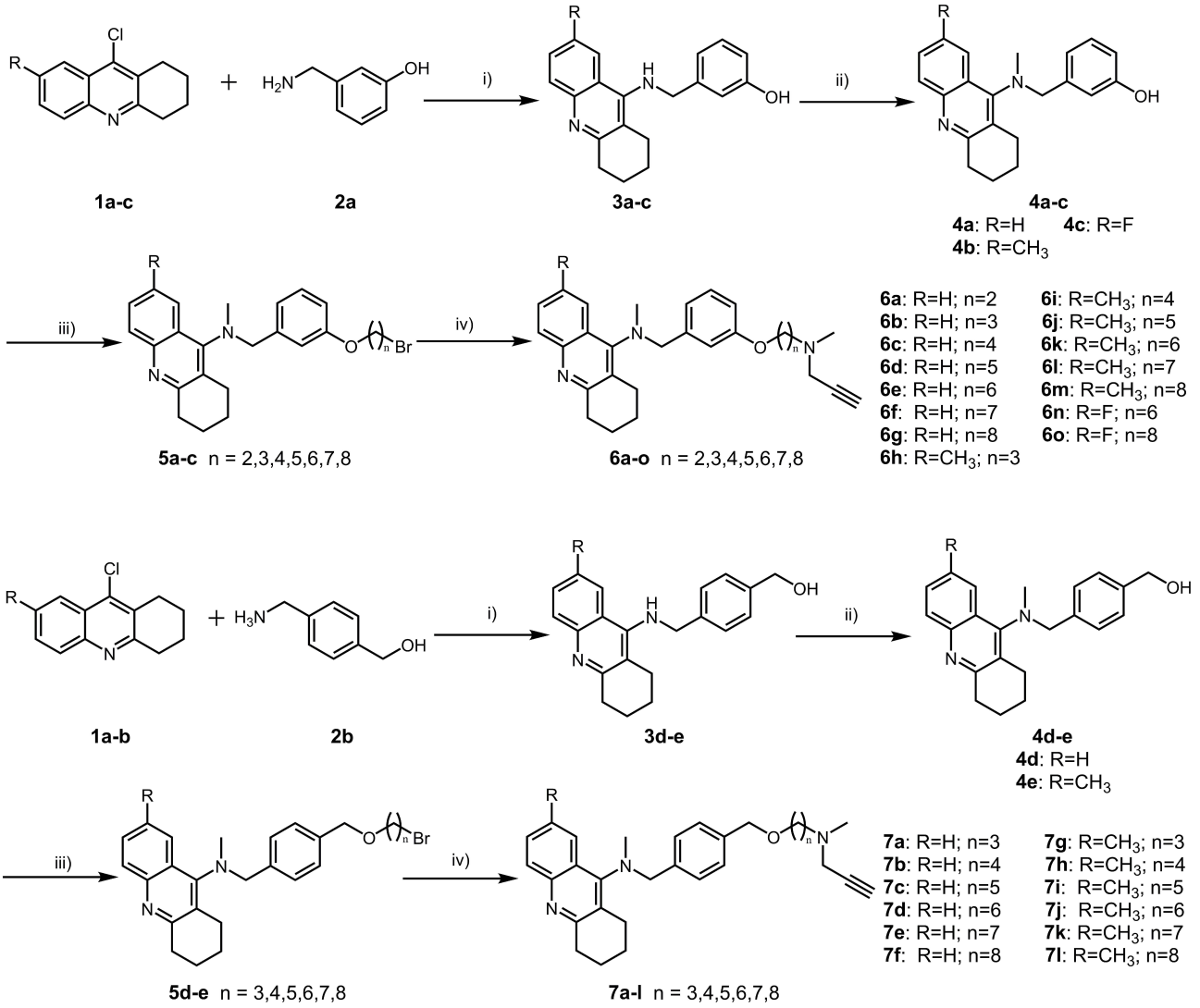

Scheme 1 Synthesis of tacrine-selegiline hybrids **6a-6o** and **7a-7l**. Reagents and conditions: (i) KI, 1-pentanol, reflux at 130 °C for 10 h; (ii) HCHO, AcOH, DMF, r.t. for 60 min, followed by $NaBH_3CN$, 8 h; (iii) $Br(CH_2)nBr$, NaH, DMF, 0 °C to r.t., 12 h; (iv) *N*-methylpropargylamine, anhydrous K_2CO_3, MeCN, reflux at 70 °C for 12 h.

N-methylpropargylamine under the alkaline condition at 70 °C.[21] The target compounds were characterized by proton NMR carbon, NMR and high resolution mass spectrometry (HRMS). However, it is noteworthy that, for the intermediates, only proton NMR and HRMS were utilized for characterization, excluding ^{13}C NMR.

In vitro Inhibition of AChE and BuChE

The inhibitory effects of all target compounds on electric eel acetylcholinesterase (*ee*AChE) and equine serum butyrylcholinesterase (*eq*BuChE) were evaluated using classical spectrophotometry as described by Ellman et al,[34] with donepezil, a well-known cholinesterase inhibitor, used as a reference compound. Additionally, in view of the high cost of human cholinesterases, only **6a-g, 7b-d** and **7h-j** hybrids, which demonstrated relatively good and balanced inhibitory activities against both *ee*AChE and *eq*BuChE, were selected for further testing on human recombinant cholinesterases from human serum (*h*AChE/*h*BuChE). The results of these experiments were expressed as IC_{50} (μM) and are summarized in Table 1.

The assays demonstrated that the majority of the compounds potently inhibited AChE and BuChE. Compounds with alkyl chains of different lengths between tacrine and *N*-methylpropargylamine were synthesized to evaluate the inhibitory activities against ChEs, as the length of the alkyl chain can influence the inhibitory ability of both AChE and BuChE.

Table 1 Inhibition of AChE and BuChE by Tacrine-Selegiline Hybrids **6a-o** and **7a-l**

Compd.	R	n	IC_{50} (μM)[a] ± SD			
			[b]eeAChE	[c]*h*AChE	[d]*eq*BuChE	[e]*h*BuChE
6a	H	2	9.02 ± 0.21	4.21 ± 0.33	2.65 ± 0.01	2.00 ± 0.02
6b	H	3	5.51 ± 0.18	2.82 ± 0.19	0.63 ± 0.01	0.41 ± 0.01
6c	H	4	12.74 ± 0.09	6.09 ± 0.05	0.94 ± 0.03	0.37 ± 0.08
6d	H	5	18.65 ± 0.04	2.6 ± 0.01	0.42 ± 0.05	0.33 ± 0.02
6e	H	6	13.83 ± 0.49	1.16 ± 0.22	0.34 ± 0.23	0.32 ± 0.04
6f	H	7	27.41 ± 0.19	1.14 ± 0.12	0.41 ± 0.18	0.31 ± 0.28
6g	H	8	28.57 ± 0.03	4.33 ± 0.02	0.84 ± 0.13	0.91 ± 0.03
6h	CH_3	3	5.36 ± 0.13	n.t.	9.90 ± 0.29	n.t.
6i	CH_3	4	5.77 ± 0.03	n.t.	11.57 ± 1.38	n.t.
6j	CH_3	5	18.18 ± 0.02	n.t.	7.25 ± 0.02	n.t.
6k	CH_3	6	36.63 ± 0.13	n.t.	6.14 ± 0.11	n.t.
6L	CH_3	7	22.96 ± 0.39	n.t.	73.89 ± 1.13	n.t.
6m	CH_3	8	32.20 ± 0.48	n.t.	130.18 ± 1.21	n.t.
6n	F	6	49.68 ± 1.11	n.t.	62.00 ± 0.41	n.t.
6o	F	8	66.31 ± 0.46	n.t.	n.a.[f]	n.t.
7a	H	3	11.86 ± 0.88	n.t.	14.15 ± 0.18	n.t.
7b	H	4	9.65 ± 0.32	2.36 ± 0.02	0.69 ± 0.03	1.47 ± 0.12
7c	H	5	13.65 ± 0.39	4.84 ± 0.45	0.89 ± 0.06	0.61 ± 0.05
7d	H	6	8.76 ± 0.12	1.57 ± 0.34	0.46 ± 0.02	0.43 ± 0.08
7e	H	7	42.12 ± 0.02	n.t.	0.19 ± 0.04	n.t.
7f	H	8	32.18 ± 0.04	n.t.	0.64 ± 0.04	n.t.
7g	CH_3	3	12.24 ± 0.01	n.t.	13.86 ± 0.06	n.t.
7h	CH_3	4	5.72 ± 0.13	16.19 ± 0.41	1.30 ± 0.03	1.78 ± 0.19
7i	CH_3	5	5.72 ± 0.28	13.41 ± 0.71	4.10 ± 0.12	1.12 ± 0.12
7j	CH_3	6	8.85 ± 0.91	45.79 ± 1.51	2.08 ± 0.11	1.27 ± 0.13
7k	CH_3	7	31.83 ± 0.21	n.t.	0.92 ± 0.03	n.t.
7L	CH_3	8	15.53 ± 0.19	n.t.	1.88 ± 0.07	n.t.
Donepezil	–	–	0.05 ± 0.002	0.04 ± 0.001	3.50 ± 0.18	2.25 ± 0.11

Notes: [a]IC_{50} values (μM) are expressed as the mean of three independent experiments ± SD. [b]eeAChE from electric eel. [c]human recombinant AChE (*h*AChE) from human serum. [d]eqBuChE from equine serum. [e]human recombinant BuChE (*h*BuChE) from human serum. [f]Compounds defined "no active" means that the percent inhibition is less than 45.0% at a concentration of 100 μM in the assay conditions.

Abbreviations: n.t, not tested; n.a, no active.

Compound **6h**, with a 3-carbon spacer, exhibited the strongest inhibitory activity against *ee*AChE (IC_{50} = 5.36 μM). For **6a-6g**, compounds containing two- and three-carbon spacers showed better *ee*AChE inhibition. For **6h-6m**, compounds with short linkers (n = 3–4) demonstrated stronger *ee*AChE inhibitory activity. Among compounds **7a-7f** and **7g-7l, 7b** (n = 4) and **7d** (n = 6), as well as **7h-7j** (n = 4–6), exhibited better *ee*AChE inhibitory activity. Furthermore, we investigated the effect of introducing different substituents at position 7 of tacrine on ChEs inhibition. As shown in Table 1, compounds with a methyl group introduced (**6i, 7h, 7i**) exhibited about 2-fold more potent *ee*AChE inhibitory activity than their corresponding unsubstituted compounds (**6c, 7b, 7c**), whereas compounds (**6h, 6j, 7g, 7j)** with the same substituent showed similar *ee*AChE inhibition as their unsubstituted counterparts (**6b, 6d, 7a, 7d**). Introduction of a fluorine atom as an electron-absorbing group at site 7 of tacrine significantly reduced the *ee*AChE inhibitory potency of the compounds (**6n-6o**). Furthermore, we explored the structure-activity relationships (SARs) of the benzene rings connecting tacrine and *N*-methylpropargylamine by comparing target compounds (**6b-6g** vs **7a-7f** and **6h-6m** vs **7g-7l**). The results suggested that compounds (**7b-7d, 7h-7j**) containing benzyl ether had higher inhibitory activity against *ee*AChE than compounds (**6c-6e, 6i-6k**) containing phenol ether. Interestingly, most compounds showed superior inhibitory activity against *h*AChE compared to *ee*AChE. However, it should be noted that the effects of different chain lengths, substituent groups at position 7 of tacrine and linked benzene ring on the inhibitory activity of *h*AChE and *ee*AChE were not completely consistent. Compounds (**6d, 6e**) containing phenol ether inhibited *h*AChE more strongly than the corresponding compounds (**7c, 7d**) containing benzyl ether. Among **6a-6g**, the long linker compounds **6e** and **6f** (n = 6–7) demonstrated relatively strong *h*AChE inhibition. The unsubstituted compound (**7b-7d**) exhibited better *h*AChE inhibitory activity than the corresponding compounds (**7h-7j**) with an introduced methyl group. In general, compounds with 4 to 8 carbon spacers demonstrated stronger *eq*BuChE inhibitory activity, and this SAR was found in compounds **6a-6g, 7a-7f** and **7g-7l**. Compound **7e** was the best *eq*BuChE inhibitor in this series of hybrids with an IC_{50} value of 0.19 μM, approximately 18-fold more potent than the reference compound donepezil (*eq*BuChE: IC_{50} = 3.50 μM). Introducing a methyl or fluorine atom at position 7 of tacrine significantly reduced the inhibitory activity of compounds toward *eq*BuChE (**6b-6g** vs **6h-6m** vs **6n-6o** and **7a-7f** vs **7g-7l**). When the chain length between tacrine and *N*-methylpropargylamine was consistent, the change of the linked benzene ring had little effect on the inhibitory activity of *eq*BuChE for the compounds without substitution at site 7 of tacrine. However, for the methyl-substituted compounds, compounds (**7h-7l**) containing benzyl ether exhibited stronger *eq*BuChE inhibitory activity than the corresponding compounds (**6i-6m**) containing phenol ether. The SARs of the effects of changes in alkyl chain length, substituent at position 7 of tacrine moiety, and the linked benzene ring on the inhibitory activity of *h*BuChE were similar to those of *eq*BuChE. Among them, compound **6f** (*h*BuChE: IC_{50} = 0.31 μM) showed the best inhibitory activity against *h*BuChE activity, approximately 7-fold stronger than donepezil (*h*BuChE: IC_{50} = 2.25 μM).

Considering the results of both human and eel cholinesterase assays, several of the hybrids demonstrated a favorable balance of AChE/BuChE inhibitory activities. Notably, **7d** showed the best balance inhibition of the two esterases, with IC_{50} values of 8.76 μM for *ee*AChE, 1.57 μM for *h*AChE, 0.46 μM for *eq*BuChE, and 0.43 μM for *h*BuChE. Therefore, this hybrid may have greater potential for the treatment of AD.

In vitro Inhibition of hMAO-A and hMAO-B

To study the multifunctional biological properties of the hybrids, we evaluated their inhibitory activities against both human recombinant MAO-A and MAO-B from human serum (*h*MAO-A and *h*MAO-B) by an Amplex Red fluorescence assay.[35] Iproniazid, an irreversible non-selective MAO-A inhibitor, and rasagiline, an irreversible selective MAO-B inhibitor, served as control drugs. AD patients often exhibit symptoms of depression, which are even considered a risk factor for the onset of AD.[33] Moreover, MAO-A can also impact the regulation of neurotransmitters in the brain; hence, dual inhibition of MAO-A and MAO-B, rather than just inhibiting MAO-B alone, may hold therapeutic value for AD.[22] Table 2 showed that most of the synthesized compounds exhibited potent inhibitory effects against both MAO-A and MAO-B. Importantly, all compounds except for **6n** and **6o** (IC_{50} values of 65.61 and 71.39 μM for *h*MAO-B, respectively) showed stronger anti-MAO-B activity (IC_{50} ranging from 1.12 to 5.78 μM) than iproniazid (IC_{50} = 7.54 μM), though weaker than rasagiline (IC_{50} = 0.23 μM). Of all the synthetic compounds, **7l** (IC_{50} = 0.22 μM for *h*MAO-A) and **6m** (IC_{50} = 1.12 μM for *h*MAO-B), with eight alkyl chains between tacrine and *N*-methylpropargylamine, exhibited

Table 2 Inhibition of *h*MAO-A and *h*MAO-B by Tacrine-Selegiline Hybrids **6a-o** and **7a-l**

Compd.	R	n	IC_{50} (μM)[a] ± SD	
			***h*MAO-A**	***h*MAO-B**
6a	H	2	10.28 ± 0.46	2.94 ± 0.19
6b	H	3	5.25 ± 0.72	2.56 ± 0.56
6c	H	4	5.67 ± 0.04	2.73 ± 0.01
6d	H	5	6.01 ± 0.03	2.84 ± 0.05
6e	H	6	4.79 ± 0.02	2.24 ± 0.07
6f	H	7	7.68 ± 0.16	2.47 ± 0.02
6g	H	8	8.89 ± 0.01	3.04 ± 0.13
6h	CH_3	3	8.73 ± 0.01	2.57 ± 0.03
6i	CH_3	4	6.54 ± 0.01	2.43 ± 0.02
6j	CH_3	5	2.83 ± 0.19	1.53 ± 0.09
6k	CH_3	6	4.87 ± 0.02	1.43 ± 0.03
6L	CH_3	7	8.15 ± 0.15	4.63 ± 1.17
6m	CH_3	8	5.74 ± 0.02	1.12 ± 0.03
6n	F	6	50.67 ± 1.24	65.61 ± 1.12
6o	F	8	61.33 ± 2.11	71.39 ± 1.34
7a	H	3	11.23 ± 0.80	5.29 ± 0.41
7b	H	4	13.77 ± 0.01	4.70 ± 0.02
7c	H	5	3.44 ± 0.34	3.14 ± 0.26
7d	H	6	2.30 ± 0.03	4.75 ± 0.24
7e	H	7	7.46 ± 0.03	5.13 ± 0.06
7f	H	8	8.29 ± 0.02	5.78 ± 0.81
7g	CH_3	3	6.57 ± 0.26	2.17 ± 0.08
7h	CH_3	4	0.62 ± 0.19	3.42 ± 0.04
7i	CH_3	5	0.53 ± 0.02	3.77 ± 0.12
7j	CH_3	6	0.30 ± 0.01	3.65 ± 0.01
7k	CH_3	7	1.11 ± 0.02	4.56 ± 0.87
7l	CH_3	8	0.22 ± 0.02	4.21 ± 0.04
Rasagiline	-	-	21.32 ± 0.01	0.23 ± 0.03
Iproniazid	-	-	7.12 ± 0.31	7.54 ± 0.23

Notes: [a]IC_{50} values (μM) for inhibition of human recombinant MAO-A or MAO-B from human serum. Values are expressed as the mean of three independent experiments ± SD.

the strongest inhibitory potency against MAO-A and MAO-B, respectively. Analysis of the MAO-A inhibitory activities of **6a-6g, 6h-6m, 7a-7f** and **7g-7l** showed that compounds with a linker length of 5 or 6 carbon atoms, such as **6e, 6j-k, 7c-d** and **7i-j** were potent MAO-A inhibitors, with some demonstrating sub-micromolar activity (eg, **7i-7j**). The introduction of a methyl group at position 7 of tacrine had little impact on the MAO-A inhibition characteristics of compounds (**6b-g** vs **6h-m**) containing phenol ether; however, it greatly increased the inhibitory effect of MAO-A of compounds (**7a-f** vs.**7g-l**) containing benzyl ether. Notably, a fluorine substitution at position 7 of tacrine significantly reduced the inhibitory properties of MAO-A (eg, **6n**: IC_{50} = 50.67 μM, **6o**: IC_{50} = 61.33 μM). Additionally, compounds (**7c-7f, 7g-7l**) containing benzyl ether showed stronger inhibitory activity against MAO-A than the corresponding compounds (**6d-6g, 6h-6m**) containing phenol ether. Furthermore, we discussed the SARs of changes in chain length, substituent at position 7 of tacrine moiety, and linked benzene ring on the inhibitory activity of MAO-B. The extension of the carbon chain did not significantly alter the IC_{50} value of MAO-B inhibition for compounds **6a-6g** (n = 2–8), and similar SARs were observed for **6h-6m, 7a-7f**, and **7g-7l**. With a few exceptions, introducing a methyl group at site 7 of tacrine enhanced the inhibitory effect on MAO-B. However, the introduction of a fluorine atom significantly decreased the MAO-B inhibitory activity, similar to that of MAO-A. Overall, compounds containing phenol ether exhibited higher

inhibitory effects on MAO-B than the corresponding compounds containing benzyl ether, which is the opposite trend compared to that of MAO-A.

Considering the above findings, **7d** was selected as the representative compound in this series of hybrids for further study due to its well-balanced and excellent inhibitory effect on ChEs and MAOs.

Molecular Docking of 7d with hAChE and hBuChE

Based on the results obtained from the in vitro inhibition of cholinesterase, it was observed that, except for compound **7h-7j**, the inhibitory activities of the other compounds (**6a-6g** and **7b-7d**) on electric eel cholinesterases were similar to those observed on human recombinant cholinesterases. Consequently, selecting the less expensive cholinesterases from electric eel for the preliminary screening of compound activity was representative, with the final results being determined based on inhibitory activities on human cholinesterases. Thus, to determine the capacity of compound **7d** targeting cholinesterase at the Molecular level, we selected the crystal structure of *h*AChE and *h*BuChE for conducting molecular docking studies using the Molecular Operating Environment (MOE) 2015.10 version software from the Canadian Chemical Computing Group. Based on the results in Figure 2A and C, compound **7d** occupies the CAS, the mid-gorge site, and the PAS of the entire *h*AChE enzyme. Specifically, the *N*-methylpropargylamine moiety of **7d** can act on the PAS of AChE and binds to Trp286 through hydrophobic interaction. The benzene ring of the benzylamine unit

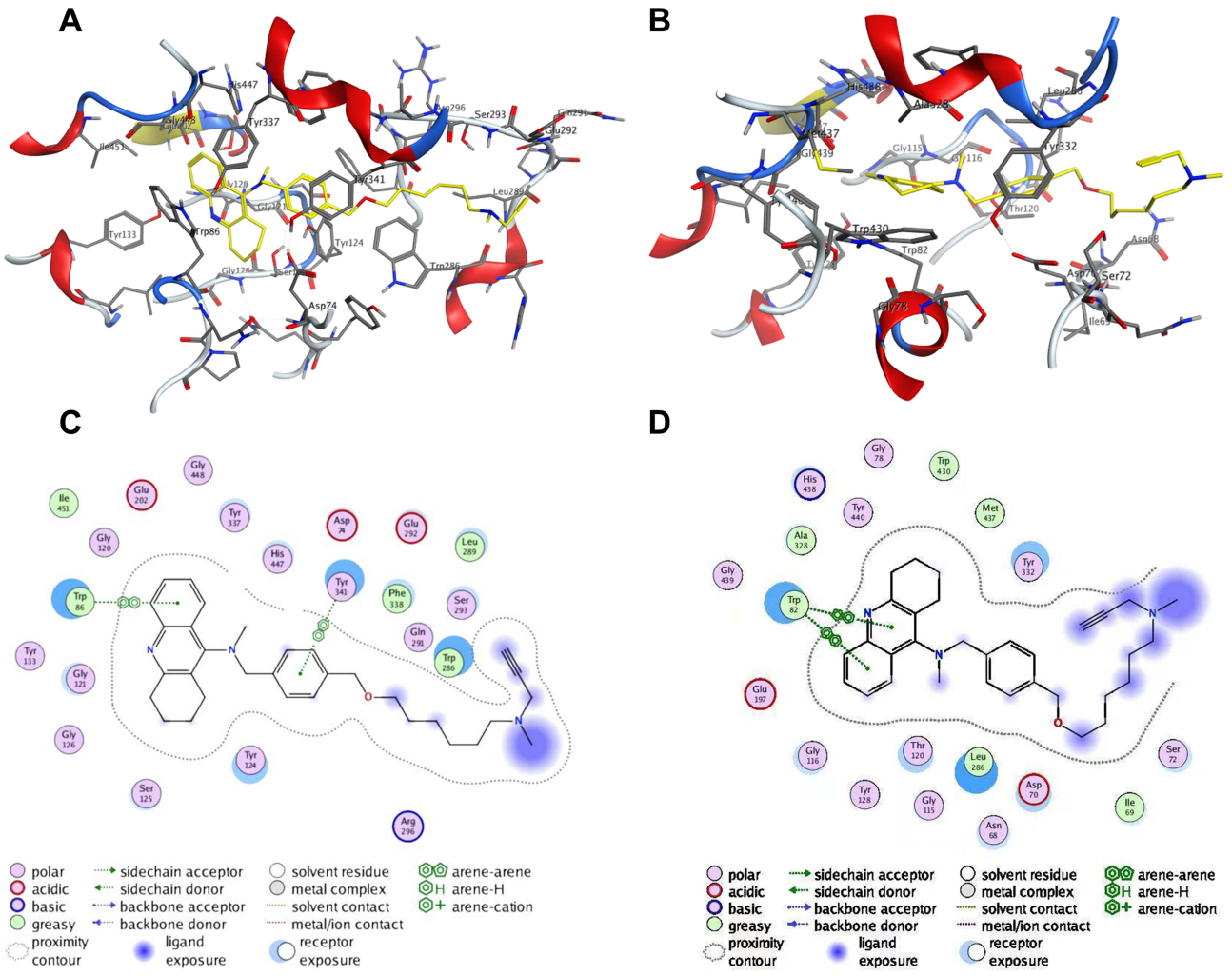

Figure 2 Molecule docking results: (**A** and **C**) were 3D and 2D docking models of compound **7d** with *h*AChE; (**B** and **D**) were 3D and 2D docking models of compound **7d** with *h*BuChE. Atom colors: yellow-carbon atoms of **7d**, grey-carbon atoms of residues of *h*AChE or *h*BuChE, dark blue-nitrogen atoms, and red-oxygen atoms. The figure was prepared using the ligand interactions application in MOE.

establishes π-π stacking interaction with Trp341, and the alkyl chain shows a hydrophobic interaction with Phe338 at the aromatic gorge. Moreover, the tacrine ring binds to the CAS through π-π stacking formed by its benzene ring with Trp86. The above docking results indicated that compound **7d** is a two-site inhibitor of the AChE, capable of binding to the CAS and PAS simultaneously. From the docking results of compound **7d** and *h*BuChE (Figure 2B and D), it can be seen that the cavity of BuChE can also be occupied by compound **7d**. In the *h*BuChE-**7d** complex, the tacrine ring establishes two π-π stacking interactions with Trp82 and binds to Ala328 and His438 through hydrophobic interaction. Additionally, the benzyl ether unit forms hydrophobic interactions with Tyr332, Thr120, and Leu286.

Molecular Docking of 7d with hMAO-B

To clearly explain the binding mode of compound **7d** and *h*MAO-B, we performed molecular docking studies using MOE software. As shown in Figure 3A and B, compound **7d** can enter the substrate cavity of MAO-B, and the tacrine ring establishes a π-H interaction with Tyr398 of the flavin adenine dinucleotide (FAD) cofactor and forms a hydrophobic interaction with Phe343, Tyr60, and Tyr435. The *N*-methylpropargylamine unit occupies the entrance cavity of the enzyme and interacts with Pro102, Pro104, Ile316, Phe168, Leu167, Leu164, Trp199 and Phe103 via van der Waals and hydrophobic forces. The results also suggested that the inhibition of MAO-B by compound **7d** may be affected by the length of the alkylene chain.

In vitro Blood–Brain Barrier Permeation

One of the main requirements for anti-AD drugs is good brain permeability to reach the target site of AD located in the CNS. Therefore, screening the ability of target compounds to infiltrate the brain is of great significance. We used the parallel artificial membrane permeability assay (PAMPA) described by Di et al, which has the advantages of simplicity, speed, and high accuracy, to investigate the blood-brain barrier (BBB) permeability of tacrine-selegiline hybrids **6a-o** and **7a-l**.[37] 10 commercially available drugs with reported values were used as reference compounds (Table 3). From the measured results, the plot of experimental data and bibliographic values for the 10 control drugs provided a good linear correlation: P_e (exp.) = 1.0654 P_e (bibl.) + 0.1625 (R^2 = 0.9967) (Figure 4). Based on the equation described above and followed the criteria established by Di et al for BBB permeability, we classified compounds as follows: P_e ($\times 10^{-6}$ cm/s) > 4.42 represented high BBB permeation predicted (CNS+), P_e ($\times 10^{-6}$ cm/s) < 2.29 represented low BBB permeation predicted (CNS-), 2.29 < P_e ($\times 10^{-6}$ cm/s) < 4.42 represented uncertain BBB permeation (CNS±). The permeability and predicted CNS penetration for all target hybrids are shown in Table 4. Notably, with the exception of compounds **6e** and **7l**, the P_e values of the remaining compounds were greater than 4.42 ($\times 10^{-6}$ cm/s), indicating that they were able to cross the BBB via passive diffusion and potentially exert biological effects in the central nervous system.

In vitro Cytotoxicity and in vivo Acute Toxicity Evaluation

The cytotoxicity of compound **7d** was evaluated in PC12 and BV-2 cells using donepezil as a positive control. The cells were exposed to different concentrations of compound **7d** for 24 hours, and cell viability was assessed by the Cell Counting Kit-8 (CCK-8) assay (Figure 5A and B).[38] Our results showed that, within a concentration range of 0.325 to 2.5 μM, compound **7d** had no significant effect on the viability of either cell line, which was comparable to the toxicity of donepezil. However, at higher concentrations (above 2.5 μM), we observed a decrease in cell viability, with some variability between the two cell lines. Notably, at a concentration of 10 μM, the cytotoxicity of **7d** to BV-2 cells surpassed 50%. Therefore, compound **7d** has moderate in vitro cellular safety.

To assess the safety of compound **7d** in vivo, an acute toxicity study was performed using KM mice (20–24 g, 10 mice per group, half male and half female). We administered compound **7d** orally at doses of 625, 1250 and 2500 mg/kg[36,38,39] and monitored the mice for 4 h for any signs of death, abnormal behavior, or dietary changes. No such effects were observed in any of the animals. We also recorded the body weights of all mice in the control and treatment groups for 14 days after a single-dose administration. Our results showed that the mice in all groups exhibited a gradual increase in body weight, and the average weight change in the low, middle, and high dose groups was comparable to that in the control group, indicating no obvious acute toxicity (Figure 6). To further evaluate the potential of compound **7d** to cause tissue damage, we observed paraffin sections of tissues

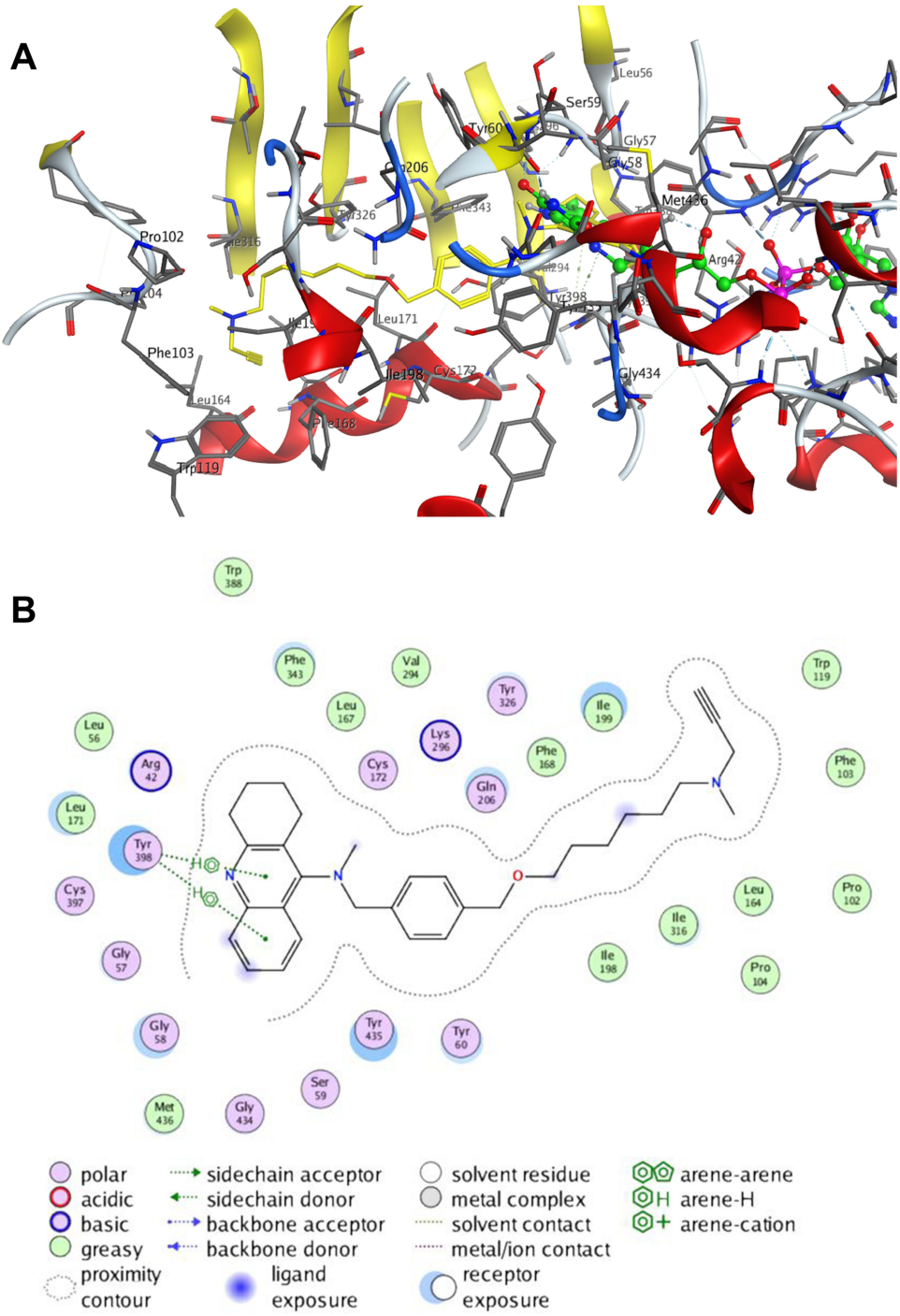

Figure 3 Molecule docking results: (**A**) 3D docking model of compound **7d** with *h*MAO-B. Atom colors: yellow-carbon atoms of **7d**, grey-carbon atoms of residues of *h*MAO-B, green-carbon atoms of FAD, dark blue-nitrogen atoms, and red-oxygen atoms; (**B**) 2D schematic diagram of docking model of compound **7d** with *h*MAO-B. The figure was prepared using the ligand interactions application in MOE.

(heart, liver, kidney, lung and brain) from mice that had been treated with vehicle (control group) or compound **7d** (2500 mg/kg) for 14 days. Hematoxylin-eosin (HE) staining revealed no obvious signs of tissue damage in the treated mice, indicating that compound **7d** was well tolerated at the dosage of 2500 mg/kg (Figure 7).

Table 3 Permeability P_e (× 10^{-6} Cm/s) in the PAMPA-BBB Assay for 10 Commercial Drugs in the Experiment Validation

Commercial Drugs	Bibliography[a]	Experiment[b]
Testosterone	17.0	18.45 ± 0.13
Estradiol	12.0	13.17 ± 0.34
Progesterone	9.3	9.78 ± 0.19
Chlorpromazine	6.5	7.12 ± 0.22
Caffeine	1.3	2.10 ± 0.23
Corticosterone	5.1	4.90 ± 0.11
Hydrocortisone	1.9	2.10 ± 0.24
Ofloxacin	0.8	0.99 ± 0.08
Atenolol	0.8	0.80 ± 0.07
Theophylline	0.1	0.60 ± 0.23

Notes: [a]Taken from Ref.[37] [b]Experimental data are expressed as mean ± SD from three independent experiments, using PBS: EtOH (70:30) as solvent.

In vivo Efficacy Study

Given the promising in vitro pharmacological activity and in vitro and in vivo safety of compound **7d**, we next selected the scopolamine-induced memory impairment mouse model as the AD animal model for the step-down passive avoidance assay. Using donepezil as a positive control to determine whether **7d** could improve the cognitive deficit in vivo.[38,40,41] The experimental results (Figure 8A and B) showed that compared to the control group, the model group had significantly shorter latency (Tukey's post hoc test, $p < 0.0001$) and a higher number of errors (Kruskal–Wallis test, $p < 0.0001$), indicating the successful establishment and reliability of the AD model. Administration of compound **7d** could prolong the latency and reduce the number of errors in mice in a dose-dependent manner. Compared with donepezil, the high-dose group of compound **7d** (20 mg/kg) exhibited longer latency and fewer errors, while the medium-dose group (10 mg/kg) showed the similar number of errors and latency. Additionally, although the latency (Tukey's post hoc test, $p = 0.01476$) and the number of errors (Kruskal–Wallis test, $p = 0.2219$) in the low-dose group (5 mg/kg) were not statistically significant compared to the model group, improvements were observed in both. In summary, consistent with the expected results, compound **7d** could cross the BBB and act on targets in the CNS, leading to the reversal of memory impairment.

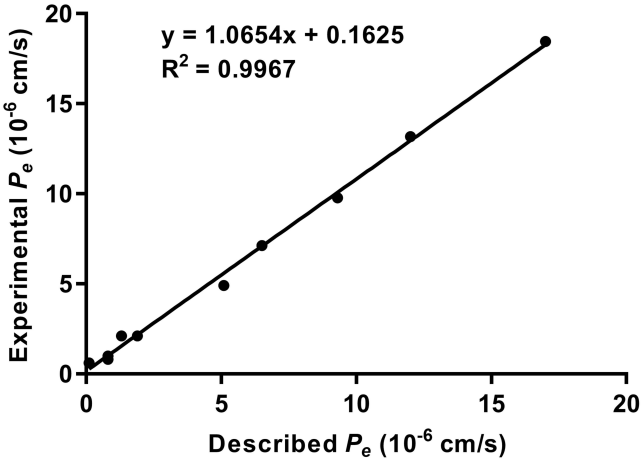

Figure 4 Lineal correlation between experimental and reported permeability of commercial drugs using the PAMPA-BBB assay. P_e (exp.) = 1.0654 P_e (bibl.) + 0.1625 (R^2 = 0.9967).

Table 4 Permeability P_e (× 10^{-6} Cm/s) in the PAMPA-BBB Assay for the Target Compounds and Their Predicted Penetration into CNS

Compd.	P_e (× 10^{-6}cm/s)[a]	Prediction[b]
6a	5.34 ± 0.07	CNS+
6b	6.88 ± 0.23	CNS+
6c	5.89 ± 0.35	CNS+
6d	4.88 ± 0.27	CNS+
6e	4.04 ± 0.11	CNS±
6f	6.10 ± 0.67	CNS+
6g	7.13 ± 0.56	CNS+
6h	6.50 ± 0.33	CNS+
6i	5.62 ± 0.19	CNS+
6j	6.17 ± 0.56	CNS+
6k	7.18 ± 0.34	CNS+
6L	8.23 ± 0.22	CNS+
6m	7.02 ± 0.21	CNS+
6n	7.39 ± 0.41	CNS+
6o	5.17 ± 0.46	CNS+
7a	6.17 ± 0.23	CNS+
7b	7.12 ± 0.12	CNS+
7c	9.98 ± 0.14	CNS+
7d	9.79 ± 0.24	CNS+
7e	8.78 ± 0.43	CNS+
7f	7.76 ± 0.22	CNS+
7g	6.54 ± 0.08	CNS+
7h	5.64 ± 0.17	CNS+
7i	8.89 ± 0.24	CNS+
7j	7.73 ± 0.06	CNS+
7k	6.65 ± 0.37	CNS+
7l	4.33 ± 0.38	CNS±

Notes: [a]Experimental data are expressed as mean ± SD from three independent experiments, using PBS: EtOH (70:30) as solvent. [b]CNS+ is predicted as high BBB permeation with P_e (× 10^{-6} cm/s) > 4.42, CNS- is predicted as low BBB permeation with P_e (× 10^{-6} cm/s) < 2.29, CNS ± is predicted as uncertain BBB permeation with 2.29 < P_e (× 10^{-6} cm/s) < 4.42.

Pharmacokinetic Evaluation of Compound 7d

A promising candidate compound for new drugs should exhibit not only high pharmacological activity and low toxicity but also desirable pharmacokinetic (PK) properties. Initial screening of the pharmacokinetics of candidate compounds is therefore essential in the early stages of development. Taking compound **7d** as a representative, we performed pharmacokinetic studies in SD rats following intravenous (i.v.) and intraperitoneal (i.p.) administration to obtain basic pharmacokinetic parameters of compound **7d** for comprehensive evaluation. The main pharmacokinetic parameters of compound **7d** are shown in Table 5. When dosed with i.v. at 1 mg/kg, compound **7d** exhibited a reasonable peak plasma concentration (C_{max} = 465.33 μg/L) and area under the curve (AUC = 170.06 μg/L*h), with a half-life ($t_{1/2}$) of 0.82 h and a plasma clearance (CL) of 5.92 L/h/kg. Furthermore, when dosed with i.p. at 10 mg/kg, compound **7d** displayed a favorable C_{max} (364.67 μg/L) and AUC (1530.61 μg/L*h), with a suitable $t_{1/2}$ (3.16 h) and CL (6.54 L/h/kg). Additionally, the bioavailability of **7d** was up to 90.04%. These results suggested that compound **7d** possesses favorable pharmacokinetic properties.

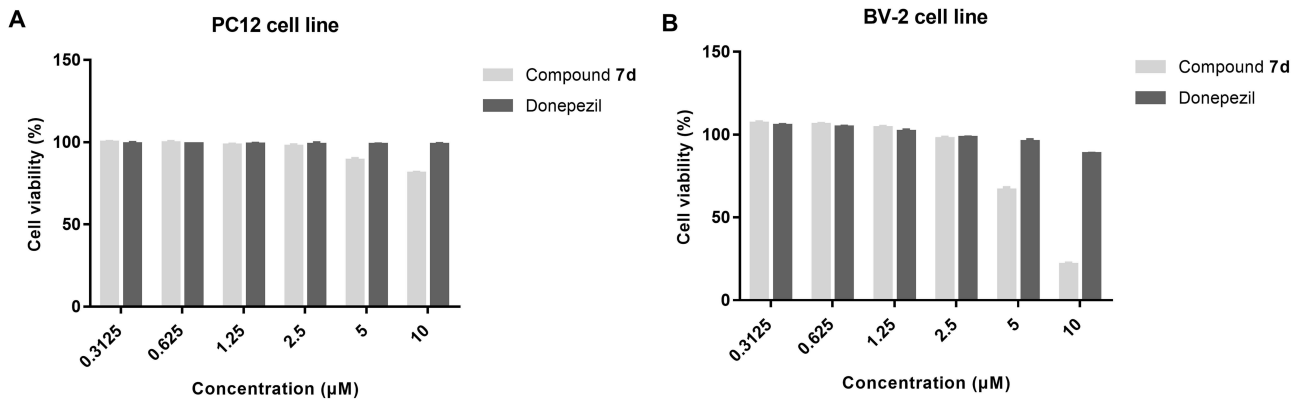

Figure 5 Cytotoxicity of compound **7d** and donepezil on (**A**) PC12 and (**B**) BV-2 cells. PC12 and BV-2 cells were incubated with different concentrations of compound **7d** or donepezil (0.3125–10 μM) for 24 h. The results were shown as cell viability after treated with compound **7d** or donepezil vs untreated control cells. Data are shown as mean ± SD of three independent experiments.

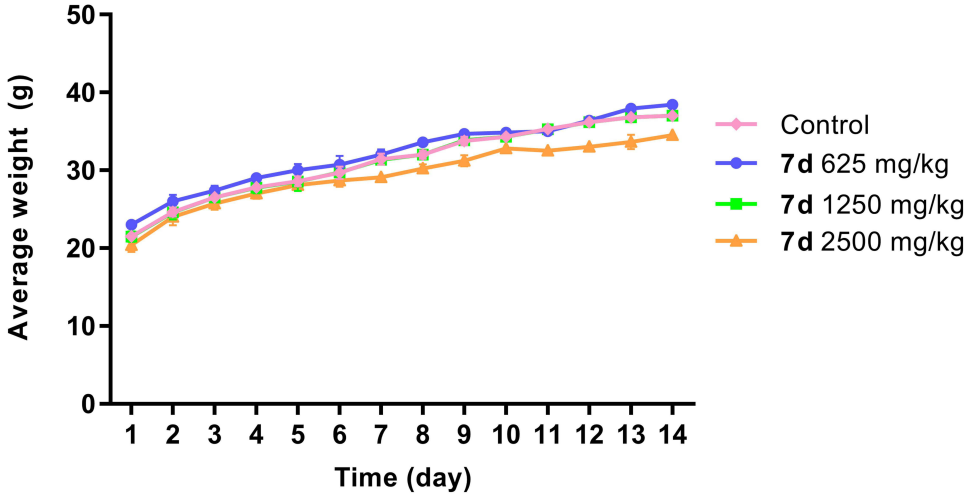

Figure 6 The change on body weight of mice after oral administration of different concentrations of compound **7d**. Data are presented as the average weight ± SD of mice (n = 10).

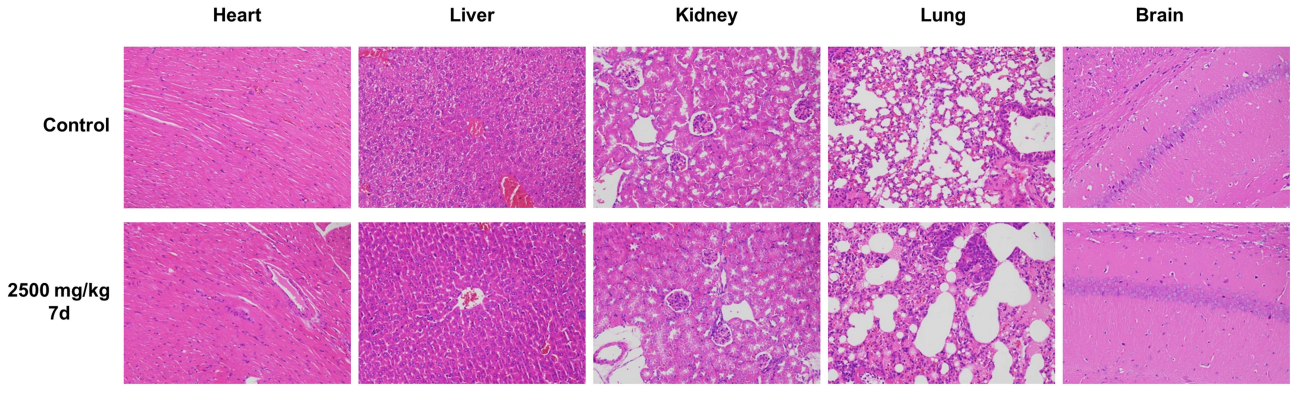

Figure 7 Histological analysis of heart, liver, kidney, lung and brain for the acute toxicity studies of compound **7d** at a dosage of 2500 mg/kg in mice. Representative images of HE-stained are shown. Bar = 200 mm.

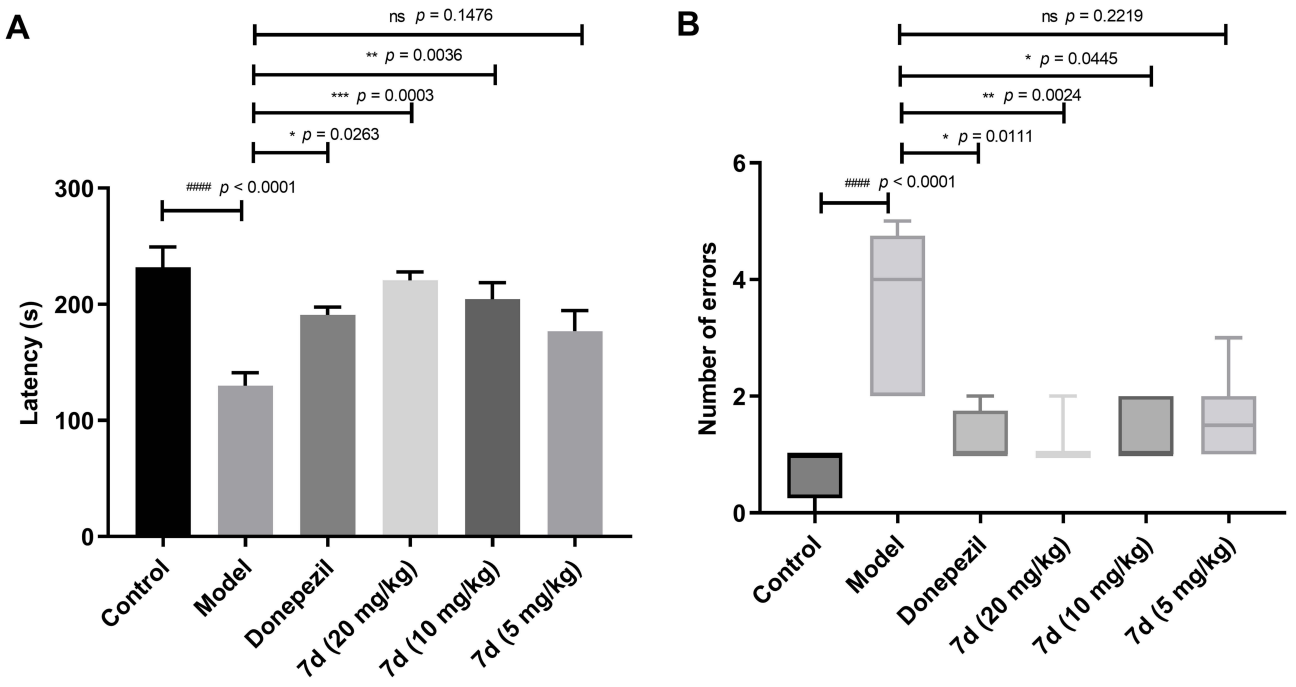

Figure 8 The effects of compound **7d** on scopolamine-induced learning and memory impairment in the step-down test. (**A**) Latency. Data were analyzed by one-way analysis of variance (ANOVA) followed by Tukey's Multiple Comparison Test, and the results are expressed as mean ± SEM (n = 8 per group). (**B**) Number of errors. Data were analyzed by the Kruskal–Wallis test followed by Dunn's Multiple Comparison Test, and the results are expressed as boxplots illustrating medians within boxes from the first quartile (25th percentile) to the third quartile (75th percentile) and whiskers ranging from minimum to maximum (n = 8 per group). A $p < 0.05$ was considered the threshold for statistical significance with 95% CI. $^{\#\#\#\#}p < 0.0001$ vs control group, $^{*}p < 0.05$, $^{**}p < 0.01$, $^{***}p < 0.001$ vs model group.

Discussion

To develop effective treatments for AD, a class of novel multifunctional hybrids, **6a-o** and **7a-l**, were designed and synthesized based on a multi-target design strategy by linking to tacrine and *N*-methylpropargylamine moiety. The ability of all target compounds to inhibit cholinesterase (ChEs) and monoamine oxidase (MAOs) was investigated. Results suggested that most of the compounds exhibited potent inhibitory activities against both enzymes in vitro. Compound **7d** showed suitable and best-balanced inhibitory activities against *h*AChE (IC_{50} = 1.57 μM), *h*BuChE (IC_{50} = 0.43 μM), *h*MAO-A (IC_{50} = 2.30 μM) and *h*MAO-B (IC_{50} = 4.75 μM). Molecular docking studies revealed that **7d** was a dual-site inhibitor of *h*AChE, while also displaying binding affinity towards *h*BuChE and *h*MAO-B. Compound **7d** presented low neurotoxicity and good in vivo safety with tolerated doses up to 2500 mg/kg while being able to cross the BBB and exert central activity. In the step-down passive avoidance test, compound **7d** significantly ameliorated memory impairment in

Table 5 Pharmacokinetic Parameters of Compound **7d** After I.v. and I.p. Administration

Parameters[a]	i.v. (1 mg/kg)	i.p. (10 mg/kg)
$T_{1/2}$ (h)	0.82 ± 0.07	3.16 ± 0.69
T_{max} (h)	0.03 ± 0.00	0.67 ± 0.29
C_{max} (μg/L)	465.33 ± 56.77	364.67 ± 223.41
$AUC_{0\text{-}inf}$ (μg/L*h)	170.06 ± 17.54	1530.61 ± 76.36
Cl (L/h/kg)	5.92 ± 0.61	6.54 ± 3.30
F (%)	-	90.04 ± 4.49

Notes: [a]Male SD rats were treated with compound **7d** by i.v. (1 mg/kg) and i.p. (10 mg/kg) administration. Data are presented as the mean ± SD (n = 3).
Abbreviations: i.v, intravenous; i.p, intraperitoneal.

a scopolamine-induced mouse model in a dose-dependent manner. Further pharmacokinetic studies showed that compound **7d** had acceptable pharmacokinetic properties after intravenous and intraperitoneal administration.

However, it should be noted that this study has a limitation in that although tacrine-selegiline hybrids **6a-o** and **7a-l** were characterized by ^{1}H NMR, ^{13}C NMR and HRMS, the intermediates were only characterized by ^{1}H NMR and HRMS, excluding ^{13}C NMR. In fact, from a rigorous standpoint, it would be advantageous to have carbon NMR characterization for the new intermediates.

Conclusion

Based on the above findings, compound **7d** could be a promising multi-target agent for further investigation as a potential treatment for AD.

Supporting Information

The ^{1}H NMR and HRMS spectra of intermediates 3a-e, 4a-4e, as well as the ^{1}H NMR, ^{13}C NMR, HRMS spectra and HPLC analysis of the target compounds 6a-o, 7a-l, were available as Supporting Information.

Ethical Approval

All animal work was carried out in accordance with the institutional guidelines for animal care and use and was approved by the Ethical Committee at Guangxi Medical University Cancer Hospital (Approval LW2023114, date 10/01/2023).

Acknowledgments

This work is supported by the Guangxi Science Fund for Distinguished Young Scholars (Grant No. 2022GXNSFFA035030), the Special Funds for Science and Technology Development under the Guidance of the Central Government (Grant No. ZY20198020), the National Natural Science Foundation of China (Grant Nos. 31970371, 31600265), the Open Project Program of Guangxi Key Laboratory of Brain and Cognitive Neuroscience (Guilin Medical University, GKLBCN-202301-02), the Guangxi Medical University Training Program for Distinguished Young Scholars, the Guangxi Postdoctoral Research Fund.

Author Contributions

All authors made a significant contribution to the work reported, whether that is in the conceptualization, study design, execution, acquisition of data, analysis and interpretation, or in all these areas; took part in drafting, revising or critically reviewing the article; gave final approval of the version to be published; have agreed on the journal to which the article has been submitted; and agree to be accountable for all aspects of the work.

Disclosure

The authors report no conflicts of interest in this work.

References

1. Alzheimer's A. 2016 Alzheimer's disease facts and figures. *Alzheimers Dement*. 2016;12:459–509. doi:10.1016/j.jalz.2016.03.001
2. Scheltens P, De Strooper B, Kivipelto M, et al. Alzheimer's disease. *Lancet*. 2021;397:1577–1590. doi:10.1016/S0140-6736(20)32205-4
3. Collaborators GDF. Estimation of the global prevalence of dementia in 2019 and forecasted prevalence in 2050: an analysis for the global burden of disease study 2019. *Lancet Public Health*. 2022;7:105–125. doi:10.1016/s2468-2667(21)00249-8
4. Levey AI. Progress with Treatments for Alzheimer's Disease. *N Engl J Med*. 2021;384:1762–1763. doi:10.1056/NEJMe2103722
5. Li Q, Xing S, Chen Y, et al. Discovery and biological evaluation of a novel highly potent selective butyrylcholinsterase inhibitor. *J Med Chem*. 2020;63:10030–10044. doi:10.1021/acs.jmedchem.0c01129
6. Scarpini E, Scheltens P, Feldman H. Treatment of Alzheimer's disease: current status and new perspectives. *Lancet Neurol*. 2003;2:539–547. doi:10.1016/s1474-4422(03)00502-7
7. Ballard C, Gauthier S, Corbett A, Brayne C, Aarsland D, Jones E. Alzheimer's disease. *Lancet*. 2011;377:1019–1031. doi:10.1016/s0140-6736(10)61349-9
8. Chun H, Im H, Kang YJ, et al. Severe reactive astrocytes precipitate pathological hallmarks of Alzheimer's disease via H(2)O(2)(-) production. *Nat Neurosci*. 2020;23:1555–1566. doi:10.1038/s41593-020-00735-y

9. Simunkova M, Alwasel SH, Alhazza IM, et al. Management of oxidative stress and other pathologies in Alzheimer's disease. *Arch Toxicol*. 2019;93:2491–2513. doi:10.1007/s00204-019-02538-y
10. Vaz M, Silvestre S. Alzheimer's disease: recent treatment strategies. *Eur J Pharmacol*. 2020;887:173554. doi:10.1016/j.ejphar.2020.173554
11. Høilund-Carlsen PF, Revheim ME, Costa T, et al. Passive Alzheimer's immunotherapy: a promising or uncertain option? *Ageing Res Rev*. 2023;90:101996. doi:10.1016/j.arr.2023.101996
12. Przybyłowska M, Kowalski S, Dzierzbicka K, Inkielewicz-Stepniak I. Therapeutic Potential of Multifunctional Tacrine Analogues. *Curr Neuropharmacol*. 2019;17:472–490. doi:10.2174/1570159x16666180412091908
13. Perry EK, Tomlinson BE, Blessed G, Bergmann K, Gibson PH, Perry RH. Correlation of cholinergic abnormalities with senile plaques and mental test scores in senile dementia. *Br Med J*. 1978;2:1457–1459. doi:10.1136/bmj.2.6150.1457
14. Kucukoglu K, Gul HI, Taslimi P, Gulcin I, Supuran CT. Investigation of inhibitory properties of some hydrazone compounds on hCA I, hCA II and AChE enzymes. *Bioorg Chem*. 2019;86:316–321. doi:10.1016/j.bioorg.2019.02.008
15. Li Q, Yang H, Chen Y, Sun H. Recent progress in the identification of selective butyrylcholinesterase inhibitors for Alzheimer's disease. *Eur J Med Chem*. 2017;132:294–309. doi:10.1016/j.ejmech.2017.03.062
16. Gómez-Ramos P, Morán MA. Ultrastructural localization of butyrylcholinesterase in senile plaques in the brains of aged and Alzheimer disease patients. *Mol Chem Neuropathol*. 1997;30:161–173. doi:10.1007/bf02815095
17. Dogterom P, Nagelkerke JF, Mulder GJ. Hepatotoxicity of tetrahydroaminoacridine in isolated rat hepatocytes: effect of glutathione and vitamin E. *Biochem Pharmacol*. 1988;37:2311–2313. doi:10.1016/0006-2952(88)90356-5
18. Zemek F, Drtinova L, Nepovimova E, et al. Outcomes of Alzheimer's disease therapy with acetylcholinesterase inhibitors and memantine. *Expert Opin Drug Saf*. 2014;13:759–774. doi:10.1517/14740338.2014.914168
19. Nepovimova E, Korabecny J, Dolezal R, et al. Tacrine-trolox hybrids: a novel class of centrally active, nonhepatotoxic multi-target-directed ligands exerting anticholinesterase and antioxidant activities with low in vivo toxicity. *J Med Chem*. 2015;58:8985–9003. doi:10.1021/acs.jmedchem.5b01325
20. Tumiatti V, Minarini A, Bolognesi ML, Milelli A, Rosini M, Melchiorre C. Tacrine derivatives and Alzheimer's disease. *Curr Med Chem*. 2010;17:1825–1838. doi:10.2174/092986710791111206
21. Lu C, Zhou Q, Yan J, Du Z, Huang L, Li X. A novel series of tacrine-selegiline hybrids with cholinesterase and monoamine oxidase inhibition activities for the treatment of Alzheimer's disease. *Eur J Med Chem*. 2013;62:745–753. doi:10.1016/j.ejmech.2013.01.039
22. Finberg JP. Update on the pharmacology of selective inhibitors of MAO-A and MAO-B: focus on modulation of CNS monoamine neurotransmitter release. *Pharmacol Ther*. 2014;143:133–152. doi:10.1016/j.pharmthera.2014.02.010
23. Chen JJ, Wilkinson JR. The monoamine oxidase type B inhibitor rasagiline in the treatment of Parkinson disease: is tyramine a challenge? *J Clin Pharmacol*. 2012;52:620–628. doi:10.1177/0091270011406279
24. Kalgutkar AS, Dalvie DK, Castagnoli N, Taylor TJ. Interactions of nitrogen-containing xenobiotics with monoamine oxidase (MAO) isozymes A and B: SAR studies on MAO substrates and inhibitors. *Chem Res Toxicol*. 2001;14:1139–1162. doi:10.1021/tx010073b
25. Boppana K, Dubey PK, Jagarlapudi SA, Vadivelan S, Rambabu G. Knowledge based identification of MAO-B selective inhibitors using pharmacophore and structure based virtual screening models. *Eur J Med Chem*. 2009;44:3584–3590. doi:10.1016/j.ejmech.2009.02.031
26. Gottfries CG. Alzheimer's disease and senile dementia: biochemical characteristics and aspects of treatment. *Psychopharmacology*. 1985;86:245–252. doi:10.1007/bf00432208
27. Naoi M, Maruyama W. Monoamine oxidase inhibitors as neuroprotective agents in age-dependent neurodegenerative disorders. *Curr Pharm Des*. 2010;16:2799–2817. doi:10.2174/138161210793176527
28. Zhang P, Xu S, Zhu Z, Xu J. Multi-target design strategies for the improved treatment of Alzheimer's disease. *Eur J Med Chem*. 2019;176:228–247. doi:10.1016/j.ejmech.2019.05.020
29. Farina R, Pisani L, Catto M, et al. Structure-based design and optimization of multitarget-directed 2H-chromen-2-one derivatives as potent inhibitors of monoamine oxidase B and cholinesterases. *J Med Chem*. 2015;58:5561–5578. doi:10.1021/acs.jmedchem.5b00599
30. Schneider LS, Geffen Y, Rabinowitz J, et al. Low-dose ladostigil for mild cognitive impairment: a Phase 2 placebo-controlled clinical trial. *Neurology*. 2019;93:1474–1484. doi:10.1212/wnl.0000000000008239
31. Hiremathad A, Keri RS, Esteves AR, Cardoso SM, Chaves S, Santos MA. Novel tacrine-hydroxyphenylbenzimidazole hybrids as potential multitarget drug candidates for Alzheimer's disease. *Eur J Med Chem*. 2018;148:255–267. doi:10.1016/j.ejmech.2018.02.023
32. Frantz MC, Pellissier LP, Pflimlin E, et al. LIT-001, the first nonpeptide oxytocin receptor agonist that improves social interaction in a mouse model of autism. *J Med Chem*. 2018;61:8670–8692. doi:10.1021/acs.jmedchem.8b00697
33. Bolea I, Juárez-Jiménez J, de Los Ríos C, et al. Synthesis, biological evaluation, and molecular modeling of donepezil and N-[(5-(benzyloxy)-1-methyl-1H-indol-2-yl)methyl]-N-methylprop-2-yn-1-amine hybrids as new multipotent cholinesterase/monoamine oxidase inhibitors for the treatment of Alzheimer's disease. *J Med Chem*. 2011;54:8251–8270. doi:10.1021/jm200853t
34. Ellman GL, Courtney KD, Andres V, Feather-Stone RM. A new and rapid colorimetric determination of acetylcholinesterase activity. *Biochem Pharmacol*. 1961;7:88–95. doi:10.1016/0006-2952(61)90145-9
35. Matos MJ, Terán C, Pérez-Castillo Y, Uriarte E, Santana L, Viña D. Synthesis and study of a series of 3-arylcoumarins as potent and selective monoamine oxidase B inhibitors. *J Med Chem*. 2011;54:7127–7137. doi:10.1021/jm200716y
36. Jiang N, Huang Q, Liu J, et al. Design, synthesis and biological evaluation of new coumarin-dithiocarbamate hybrids as multifunctional agents for the treatment of Alzheimer's disease. *Eur J Med Chem*. 2018;146:287–298. doi:10.1016/j.ejmech.2018.01.055
37. Di L, Kerns EH, Fan K, McConnell OJ, Carter GT. High throughput artificial membrane permeability assay for blood-brain barrier. *Eur J Med Chem*. 2003;38:223–232. doi:10.1016/s0223-5234(03)00012-6
38. Zhong GH, Guo J, Pang CY, et al. Novel AP2238-clorgiline hybrids as multi-target agents for the treatment of Alzheimer's disease: design, synthesis, and biological evaluation. *Bioorg Chem*. 2023;130:106224. doi:10.1016/j.bioorg.2022.106224
39. He Q, Liu J, Lan JS, et al. Coumarin-dithiocarbamate hybrids as novel multitarget AChE and MAO-B inhibitors against Alzheimer's disease: design, synthesis and biological evaluation. *Bioorg Chem*. 2018;81:512–528. doi:10.1016/j.bioorg.2018.09.010
40. Ukai M, Kobayashi T, Shinkai N, Shan-Wu X, Kameyama T. Dynorphin A-(1-13) potently improves scopolamine-induced impairment of passive avoidance response in mice. *Eur J Pharmacol*. 1995;274:89–93. doi:10.1016/0014-2999(94)00710-o

41. Sang Z, Pan W, Wang K, et al. Design, synthesis and evaluation of novel ferulic acid-O-alkylamine derivatives as potential multifunctional agents for the treatment of Alzheimer's disease. *Eur J Med Chem*. 2017;130:379–392. doi:10.1016/j.ejmech.2017.02.039
42. Li Q, Meng L, Zhou S, et al. Rapid generation of novel benzoic acid-based xanthine derivatives as highly potent, selective and long acting DPP-4 inhibitors: scaffold-hopping and prodrug study. *Eur J Med Chem*. 2019;180:509–523. doi:10.1016/j.ejmech.2019.07.045
43. Xie SS, Liu J, Tang C, et al. Design, synthesis and biological evaluation of rasagiline-clorgyline hybrids as novel dual inhibitors of monoamine oxidase-B and amyloid-β aggregation against Alzheimer's disease. *Eur J Med Chem*. 2020;202:112475. doi:10.1016/j.ejmech.2020.112475
44. Jiang N, Ding J, Liu J, et al. Novel chromanone-dithiocarbamate hybrids as multifunctional AChE inhibitors with β-amyloid anti-aggregation properties for the treatment of Alzheimer's disease. *Bioorg Chem*. 2019;89:103027. doi:10.1016/j.bioorg.2019.103027